

## Article

# LGM Glaciations in the Northeastern Anatolian Mountains: New Insights

Regina Reber <sup>1,\*</sup> , Naki Akçar <sup>1</sup> , Dmitry Tikhomirov <sup>1,2</sup>, Serdar Yesilyurt <sup>1,3</sup>, Christof Vockenhuber <sup>4</sup>, Vural Yavuz <sup>5</sup>, Susan Ivy-Ochs <sup>4</sup> and Christian Schlüchter <sup>1</sup>

- <sup>1</sup> Institute of Geological Sciences, University of Bern, Baltzerstrasse 1+3, 3012 Bern, Switzerland; naki.akcar@geo.unibe.ch (N.A.); dmitry.tikhomirov@geo.uzh.ch (D.T.); yesilyurt@ankara.edu.tr (S.Y.); christian.schluechter@geo.unibe.ch (C.S.)
- <sup>2</sup> Department of Geography, University of Zurich, Winterthurerstrasse 190, 8057 Zürich, Switzerland
- <sup>3</sup> Department of Geography, Ankara University, 06230 Ankara, Turkey
- <sup>4</sup> Institute for Particle Physics, ETH Hönggerberg, Schafmattstrasse 20, 8093 Zürich, Switzerland; vockenhuber@phys.ethz.ch (C.V.); ivy@phys.ethz.ch (S.I.-O.)
- <sup>5</sup> Civil Engineering Department, Turkish-German University, 34820 Istanbul, Turkey; vural.yavuz@tau.edu.tr
- \* Correspondence: regina.reber@geo.unibe.ch

**Abstract:** Barhal Valley belongs to the Çoruh Valley System in the Kaçkar Mountains of northeastern Anatolia. This 13 km long valley is located to the south of the main weather divide and to the east of Mt. Kaçkar, with the highest peak of the mountain range being 3932 m. Today, source of an average yearly precipitation of 2000 mm of moisture is the Black Sea, situated approximately 40 km to the north of the study site. Glaciers of the Last Glacial Maximum (LGM) descended directly from Mt. Kaçkar and reached an altitude of ca. 1850 m a.s.l. (above sea level). In this study, we are exploring whether the position of Barhal Valley to the south of the main weather divide and its east–west orientation have an influence on the existence and expansion of paleoglaciers. Here, we present 32 new cosmogenic <sup>36</sup>Cl dates on erratic boulders from the Çoruh Valley System. We reconstructed three geomorphologically well-contained glacier advances in the Barhal Valley, namely at  $34.0 \pm 2.3$  ka,  $22.2 \pm 2.6$  ka, and  $18.3 \pm 1.7$  ka within the time window of the global LGM. Field evidence shows that the glacier of the  $18.3 \pm 1.7$  ka advance disappeared rapidly and that by the latest time, at  $15.6 \pm 1.8$  ka, the upper cirques were ice-free. No evidence for Lateglacial glacier fluctuations was found, and the Neoglacial activity is restricted to the cirques with rock glaciers. A range of 2700 to 3000 m for the Equilibrium Line Altitude (ELA) at the LGM was reported based on modeling of the glacial morphology. We determined that the most likely position of the LGM ELA in the Çoruh Valley System was at 2900 m a.s.l. We suggest an alternative moisture source to the direct transport from the Black Sea for the ice accumulation in the Eastern Black Sea Mountains. The shift of the Polar Front and of the Siberian High Pressure System to the south during the LGM resulted in the domination of easterly airflow to the Caucasus and Kaçkar Mountains with moisture from expanded lakes in central–western Siberia and from the enlarged Aral- and Caspian Seas.

**Keywords:** erratic boulders; cosmogenic <sup>36</sup>Cl; LGM Glaciations; eastern Anatolia; glacier retreat



**Citation:** Reber, R.; Akçar, N.; Tikhomirov, D.; Yesilyurt, S.; Vockenhuber, C.; Yavuz, V.; Ivy-Ochs, S.; Schlüchter, C. LGM Glaciations in the Northeastern Anatolian Mountains: New Insights. *Geosciences* **2022**, *12*, 257. <https://doi.org/10.3390/geosciences12070257>

Academic Editors: James A. Smith and Jesus Martinez-Frias

Received: 16 May 2022

Accepted: 20 June 2022

Published: 22 June 2022

**Publisher's Note:** MDPI stays neutral with regard to jurisdictional claims in published maps and institutional affiliations.



**Copyright:** © 2022 by the authors. Licensee MDPI, Basel, Switzerland. This article is an open access article distributed under the terms and conditions of the Creative Commons Attribution (CC BY) license (<https://creativecommons.org/licenses/by/4.0/>).

## 1. Introduction

Glaciers are the key element for the reconstruction of paleocirculation patterns and, therefore, of transport of moisture to an area, as described e.g., in [1]. Today, climate indicators such as temperature, barometric pressure, and precipitation are recorded instrumentally. However, for records of the past, these need to be extracted from gearchives. In mountain areas with sufficient elevation and precipitation, the cryosphere, which mainly comprises glaciers, provides the most sensitive archives for climate change [2]. To read these archives, fieldwork is essential, and state-of-the-art dating techniques need to be applied. Glaciers react dynamically and rapidly to physical changes to the environment,

namely to temperature, and they provide long-term records of thousand, ten thousand, and hundred thousand years, as described e.g., in [3]. The disadvantage of glacial records is their complex sedimentary structure, especially in mountainous areas. Fieldwork, therefore, can be challenging as glacial landforms and sediments in mountains are subject to gravity-induced surface reorganization and instabilities [4]. Well-preserved glacial landforms (moraines) or sediments (tills) may be rare, and careful evaluation of erratic boulders is needed with respect to their morphological stability since deposition [5].

The mountains of Turkey and their paleoclimate records constitute a critical link between the Alps, the Balkans, and the southwest Asian mountain ranges. For this reason, Anatolia is ideally located within a zone of frontal weather dynamics and seasonal oscillations in the eastern Mediterranean (Figure 3 in [6] and [7]). The Eastern Black Sea Mountain Range in northeastern Anatolia is at close proximity to the direct moisture source of the Black Sea. For example, the Kavron Valley in the Kaçkar Mountains (elevation of 3932 m and 40 km from the coast only) receives an average annual precipitation of 1784 mm, and the coastal city of Rize receives 1989 mm [8]. In contrast, Erzurum, the city located ca. 140 km from the coast and to the south of the main mountain range, receives only 676 mm. The precipitation differences between Rize at the coast, the high mountains of Kaçkar, and inland Erzurum is a typical orography-controlled situation. With the present circulation, moisture arrives directly from the Black Sea and shows a steep precipitation gradient on the southern side of the mountain range; see, e.g., [7].

Few and small relict glaciers only exist in the Kaçkar Mountains of NE Anatolia today ([9] and references therein). This is in marked contrast to the landscape during the Last Glacial Maximum when extensive valley glaciers descended at least twice from the cirque areas. We have investigated key valleys from a glacial geological point of view over the past two decades in the Kaçkar Mountains to reconstruct the past glaciers' advances (Figure 1a).

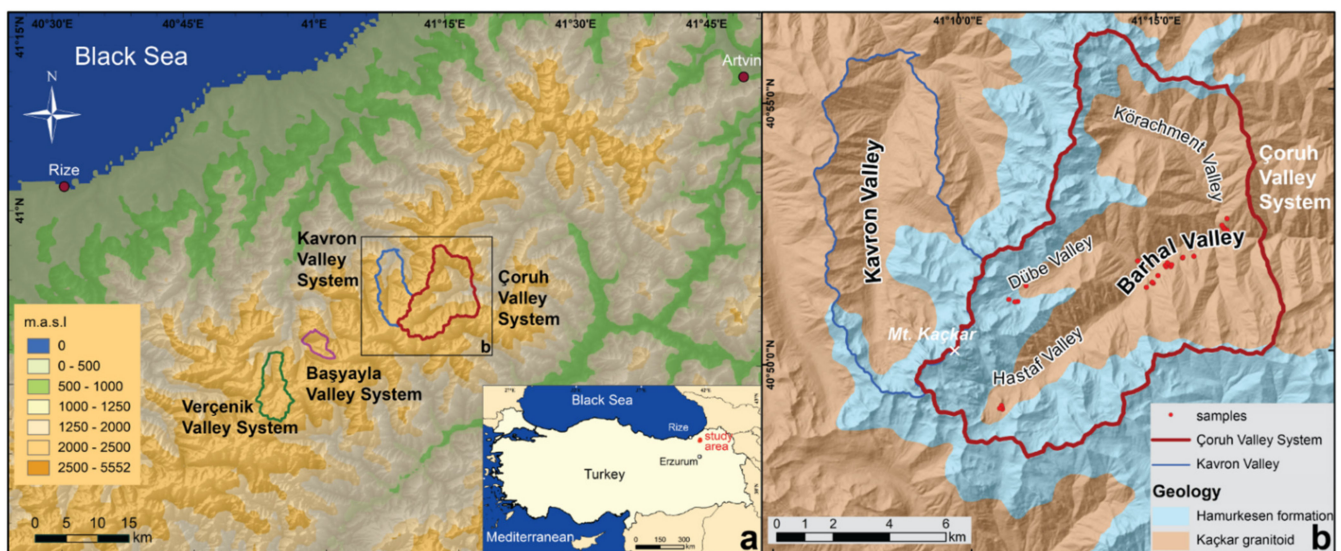


**Figure 1.** (a) Index map for the Çoruh Valley System in the Kaçkar Mountains of NE Anatolia: Kavron Valley System [10], Verçenik Valley System [11], Başyayla Valley System [12], Çoruh Valley system (this paper). (b) Neighboring Kavron and Barhal Valley descending from the highest peak of Mt. Kaçkar 3932 m. Çoruh Valley System with Hastaf, Dübe, and Körahmet tributaries, and Barhal Valley, referred to as the main valley (sample clusters red dots).

Based on literature surveys ([6] and references therein) and contacts with geologists working in the area, we started in Kavron Valley [10], followed by Verçenik Valley [11], and most recently Başyayla Valley [12]. All these valleys bear clear and extensive evidence of former glaciers with comparable chronologies from valley to valley. Kavron, Verçenik,

and Başıyayla Valleys, where our investigations were focused earlier, are open to the north and are, therefore, direct collectors of moisture moving from the Black Sea to the high Kaçkar Mountains.

The target of this study is to investigate the existence, size, and age of potential paleoglaciers to the south of the main mountain divide and, as a consequence, subject to potentially changing atmospheric circulation during glaciations (Figure 1). Additionally, it is a follow-up study of earlier investigations conducted in neighboring valleys in the north [10,11]. Therefore, the east-trending Barhal Valley, located in the southern side of the Kaçkar Mountains, was selected with a special focus on the geometry of the LGM glacier extension. Did an LGM-glaciation really occur in Barhal Valley? Additionally, then, what is the paleoclimatic context of an important glacier to the south of the main divide, but still directly connected to Mt. Kaçkar, the highest peak of the mountain range? In this study, we report field investigations, sampling campaigns, and terrestrial cosmogenic  $^{36}\text{Cl}$  analysis of the resting time of erratic boulders in Barhal Valley.

## 2. Field Area and Field Work

### 2.1. Study Area

The Barhal Valley is one of the main tributaries of the Çoruh Valley System. The uppermost part of the southwest–northeast-trending Barhal Valley is composed of three main tributaries. Yaylalar Village is at the junction of the Körahmet Valley from the north and of Hastaf Valley from the west. Olgunlar, the uppermost village, is at the junction of Dübe Valley from the north with Hastaf Valley from the west (Figures 1b and 2). Both Körahmet and Dübe Valleys are southwest–northeast trending in the upper reaches and join the main Barhal Valley after they turn to the east at right angle. Dübe and Hastaf Valleys originate in the eastern flanks of Mt. Kaçkar, the highest peak of the mountain range (Figures 1 and 2).

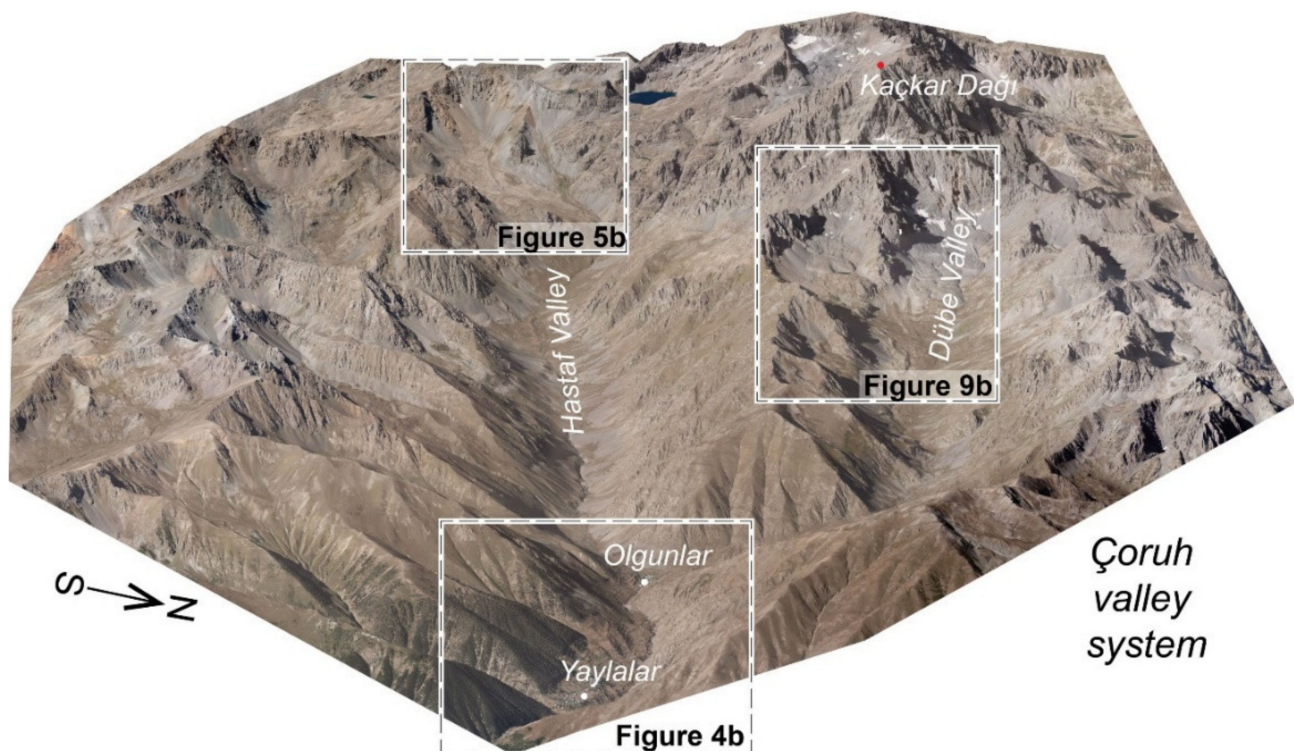


**Figure 2.** The Çoruh Valley System from an oblique aerial view based on orthophoto, to the east, and southeast of Mt. Kaçkar.

The Barhal Valley is a typical and broad U-shape valley in the sector of former glacier extensions (Figure 2). The open valley morphology ends about half a kilometer down

valley from Yaylalar Village in a gorge. The distance from the highest peak to the gorge entrance is about 13 km. The bedrock geology is complex (Figure 1b): Mt. Kaçkar is at the contact of Upper Cretaceous volcanic and volcanoclastic rocks (to the east and northeast; Hamurkesen formation, Figure 1b) and of granitic rocks of the Kaçkar composite batholith of the Late Cretaceous-Eocene age. The Kaçkar batholith complex is part of the eastern Pontide igneous terrain [13,14]. The rocks of this batholith are a wide range of quartz-rich granitoids in a complex tectonic interrelationship.

## 2.2. Sampling

Field campaigns took place in August 2010 and in August 2013. We collected a total of 31 surface samples from erratic boulder tops and one sample from a decomposing bedrock ridge beyond the extent of glaciations (Table 1) for cosmogenic surface exposure dating. After careful inspection of the boulder surface and lithology, boulder stability and its relation to an ice-contact sediment or morphology, sampling was performed using a hammer and chisel following Akçar et al. [15].

**Table 1.** Sample location and description.

Sample Name	Altitude (m)	Latitude, °N (DD.DD WGS84)	Longitude, °E (DD.DD WGS84)	Boulder Height (cm)	Sample Thickness (cm)	Shielding Correction Factor <sup>a</sup>
TRYAY-1	2310	40.85623	41.24587	100	3	0.9745
TRYAY-2	2330	40.85495	41.24291	120	3	0.9815
TRYAY-3	2990	40.81733	41.1812	140	4	0.9836
TRYAY-4	2990	40.81791	41.18103	80	3	0.9887
TRYAY-5	2980	40.81851	41.18088	80 *dh 60	3	0.9872
TRYAY-6	2990	40.81759	41.17999	100	5	0.9879
TRYAY-7	2880	40.85152	41.18879	115	3	0.9727
TRYAY-8	2905	40.85141	41.1876	100	2.5	0.9624
TRYAY-9	2960	40.85221	41.18504	160	4	0.9724
TRYAY-10	2805	40.85643	41.19236	120	3.5	0.9834
TRYAY-11	2380	40.86354	41.23956	180 *dh 50	3	0.9927
TRYAY-12	1945	40.87334	41.2763	250 *dh 40	2.5	0.9595
TRYAY-13	1940	40.8733	41.27599	400 *dh 50	3	0.9804
TRYAY-14	1910	40.87257	41.27751	200	5	0.9552
TRYAY-15	2150	40.87624	41.27764	Tor	5	0.9943
TRYAY-16	2295	40.85649	41.24531	340 *dh 160	5	0.9816
TRYAY-17	2285	40.85663	41.24546	340 *dh 80	2	0.9816
TRYAY-18	2205	40.8587	41.24792	320 *dh 100	3	0.9450
TRYAY-19	2190	40.86144	41.25145	240	4	0.9768
TRYAY-20	2155	40.86191	41.25106	280	3	0.9727
TRYAY-21	2195	40.8615	41.25346	380	2	0.9685
TRYAY-22	2180	40.86205	41.25377	260	3	0.9723
TRYAY-23	2115	40.86266	41.25207	300 *dh 200	3	0.9747
TRYAY-24	2090	40.86411	41.25843	480	3	0.9768
TRYAY-25	2090	40.86429	41.25865	270 *dh 130	3	0.9768
TRYAY-26	2115	40.86452	41.26329	290 *dh 100	5	0.9729
TRYAY-27	2005	40.86704	41.26197	640	4	0.9730
TRYAY-28	1950	40.87103	41.27026	200	3	0.9591
TRYAY-29	1935	40.87314	41.27612	200	3	0.9646
TRYAY-30	1930	40.87307	41.27623	120 *dh 40	2	0.9646
TRYAY-31	1960	40.87354	41.27586	180	2	0.9630
TRYAY-32	1990	40.87418	41.27545	340	3	0.9745

\*dh = difference in height from top of the boulder to the nearest sediment cover. <sup>a</sup> Calculated for topographic shielding and dip of the surface, following Dunne et al. [16].

## 2.3. Methodology and Lab Analytical Work

In this study, we analyzed the cosmogenic isotope <sup>36</sup>Cl because most of the suitable boulders for surface exposure dating are of volcanic lithologies. The interaction of Ca, K, Ti, Fe, and Cl in the mineral lattice of the rock surface with cosmic rays results in the production of <sup>36</sup>Cl [17,18]. We apply this physical principle to determine the exposure age of the sampled erratic boulders. As cosmogenic <sup>36</sup>Cl is produced through several production channels [19–25], we have determined the elemental composition of the whole

rock by analyzing major and trace elements on a sample aliquot at SGS Mineral Services in Toronto, Canada (Table S1). The aliquot was taken after the samples were crushed, sieved to the fraction of 0.250–0.400 mm, and leached to avoid meteoric contamination. The extraction of cosmogenic  $^{36}\text{Cl}$  was performed following a modified laboratory protocol by Akçar et al. [26]. In this protocol, only the carbonate fraction of the whole rock was dissolved. We combined nitric and hydrofluoric acids to fully dissolve the samples. Prior to dissolution, the samples were spiked with 2.5 mg of  $^{35}\text{Cl}$  to apply chlorine isotope dilution method for AMS measurement at ETH [27]. Assuming a natural ratio of  $^{35}\text{Cl}/^{37}\text{Cl}$  in the sample, the method allows determining chlorine-35, -36, and -37 concentrations, and as a result, more precise and accurate dating with  $^{36}\text{Cl}$  [28].

The concentrations of natural Cl and  $^{36}\text{Cl}$  were determined from one target at the ETH TANDEM AMS facility using the gas-filled magnet method to remove the isobar  $^{36}\text{S}$  [29,30]. The ratio of  $^{36}\text{Cl}/\text{Cl}$  was normalized to the ETH internal standard K382/4N with a value of  $17.36 \pm 0.35 \cdot 10^{-12}$  [30]. The concentration of stable Cl was calculated using a  $^{37}\text{Cl}/^{35}\text{Cl}$  ratio of 31.98% of K382/4N standard and background ratio of a machine blank. The resulting  $^{36}\text{Cl}/\text{Cl}$  ratio varies among the samples from  $0.053 \cdot 10^{-12}$  to  $0.595 \cdot 10^{-12}$ , while the ratio of the three preparation blanks has a range from  $0.002 \cdot 10^{-12}$  to  $0.005 \cdot 10^{-12}$ . The final concentrations of  $^{36}\text{Cl}$  in the rock are corrected to preparation blanks. The concentration error includes the uncertainty of the AMS standard and the blanks (Table 2).

**Table 2.** Cosmogenic nuclide data and calculated  $^{36}\text{Cl}$  exposure ages.

Sample Name	Weight of Sample	Cl Conc. in Rock (ppm)	$^{36}\text{Cl}$ Conc. ( $10^6 \text{ }^{36}\text{Cl} \text{ g(rock)}^{-1}$ )	Erosion Corrected ( $\epsilon = 1.0 \text{ mm/ka}$ ) Exposure Age (ka)
TRYAY-1	34.2269	11.45 ± 0.10	0.25 ± 0.03	16.9 ± 1.9
TRYAY-2	29.4083	26.30 ± 0.39	0.37 ± 0.02	16.8 ± 1.4
TRYAY-3	29.136	18.81 ± 0.25	0.21 ± 0.02	9.5 ± 1.0
TRYAY-4	29.0564	19.92 ± 0.13	0.44 ± 0.02	11.3 ± 0.7
TRYAY-5	27.7074	21.41 ± 0.14	0.34 ± 0.02	11.4 ± 0.9
TRYAY-6	28.6207	29.71 ± 0.15	0.92 ± 0.04	16.1 ± 0.9
TRYAY-7	28.7826	66.22 ± 0.68	0.79 ± 0.04	15.3 ± 1.3
TRYAY-8	28.6532	95.01 ± 6.46	0.92 ± 0.08	15.6 ± 1.8
TRYAY-9	30.0012	135.30 ± 0.84	1.01 ± 0.05	12.2 ± 1.2
TRYAY-10	29.1489	55.16 ± 2.59	0.78 ± 0.05	14.2 ± 1.3
TRYAY-11	29.1831	237.70 ± 9.32	1.64 ± 0.10	16.4 ± 1.8
TRYAY-12	28.4173	17.61 ± 0.26	0.41 ± 0.02	34.0 ± 2.6
TRYAY-13	34.0625	15.51 ± 0.12	0.28 ± 0.02	20.6 ± 1.7
TRYAY-14	35.4375	14.94 ± 0.09	0.15 ± 0.01	19.3 ± 1.9
TRYAY-15	28.9831	76.64 ± 1.11	0.68 ± 0.03	25.7 ± 4.0
TRYAY-16	30.1203	15.46 ± 0.17	0.16 ± 0.01	14.5 ± 1.3
TRYAY-17	30.8286	19.84 ± 0.70	0.38 ± 0.03	22.7 ± 2.0
TRYAY-18	30.3030	18.20 ± 0.29	0.48 ± 0.02	22.8 ± 1.5
TRYAY-19	30.1839	14.63 ± 0.30	0.39 ± 0.03	25.2 ± 2.2
TRYAY-20	30.1838	15.55 ± 0.10	0.40 ± 0.02	18.7 ± 1.1
TRYAY-21	30.0951	8.37 ± 0.20	0.19 ± 0.01	19.4 ± 1.7
TRYAY-22	28.0466	10.52 ± 0.32	0.19 ± 0.01	13.4 ± 1.1
TRYAY-23	27.9336	16.45 ± 0.15	0.36 ± 0.03	17.9 ± 1.5
TRYAY-24	30.3931	16.08 ± 0.11	0.37 ± 0.02	21.1 ± 1.4
TRYAY-25	30.2444	15.42 ± 0.11	0.15 ± 0.01	19.0 ± 1.9
TRYAY-26	30.2529	18.68 ± 0.24	1.31 ± 0.05	105.6 ± 8.1
TRYAY-27	30.3185	17.44 ± 0.26	0.27 ± 0.02	17.3 ± 1.6

Table 2. Cont.

Sample Name	Weight of Sample	Cl Conc. in Rock (ppm)	$^{36}\text{Cl}$ Conc. ( $10^6 \text{ }^{36}\text{Cl}$ g(rock) $^{-1}$ )	Erosion Corrected ( $\epsilon = 1.0$ mm/ka) Exposure Age (ka)
TRYAY-28	30.4064	$12.55 \pm 0.16$	$0.10 \pm 0.01$	$9.5 \pm 0.9$
TRYAY-29	30.3650	$16.47 \pm 0.24$	$0.19 \pm 0.02$	$18.8 \pm 2.1$
TRYAY-30	30.1825	$92.66 \pm 0.58$	$0.45 \pm 0.02$	$14.6 \pm 1.3$
TRYAY-31	30.2605	$15.34 \pm 0.22$	$0.45 \pm 0.02$	$25.6 \pm 1.6$
TRYAY-32	30.7316	$15.86 \pm 0.11$	$0.36 \pm 0.02$	$33.9 \pm 2.6$

Analytical errors are at the  $1\sigma$  level, including the statistical (counting) error and the combined counting uncertainty and uncertainty due to the normalization of standards and blanks. To calculate exposure ages, we used  $48.8 \pm 1.7$  atoms  $^{36}\text{Cl}$  g(Ca) $^{-1}$  a $^{-1}$  SLHL production rate from Ca spallation,  $5.3 \pm 0.5$   $^{36}\text{Cl}$  g(Ca) $^{-1}$  a $^{-1}$  SLHL production due to muon capture ([22,23], one sigma errors), and scaled after Stone [31] to 2.47 (spallation) and 1.61 (muonic) of the SLHL values. Production rate on K, 162 at g $^{-1}$  yr $^{-1}$  [32]; on Ti, 13 at g $^{-1}$  yr $^{-1}$  [33]; and on Fe, 1.9 at g $^{-1}$  yr $^{-1}$  [34]. Low-energy capture of thermal and epithermal neutrons was computed following Liu et al. [19] and Phillips et al. [21] using the production rate of epithermal neutrons above the surface  $760 \pm 150$  neutrons g $^{-1}$  a $^{-1}$  (see Alfimov and Ivy Ochs, [24]). Exposure ages are corrected for shielding of surrounding topography, and sample thickness.

For the calculation of the exposure ages, we used an in-house Matlab code based on Alfimov and Ivy-Ochs [24]. Sample-specific parameters are listed in Table 1. We used the following production rates of cosmogenic  $^{36}\text{Cl}$  by spallation: on Ca  $48.8 \pm 1.7$  atoms  $^{36}\text{Cl}$  g(Ca) $^{-1}$  a $^{-1}$  [22], on K  $162$  g $^{-1}$  yr $^{-1}$  [32], on Ti  $13$  g $^{-1}$  yr $^{-1}$  [33] and on Fe  $1.9$  g $^{-1}$  yr $^{-1}$  [34]. An attenuation length of high-energy neutrons of  $160$  g cm $^{-2}$  [16] was used together with a rock density of  $2.7$  g cm $^{-3}$ . For the production rate of epithermal and thermal neutrons in the atmosphere at the land/atmosphere interface, we used  $757$  n g $^{-1}$  yr $^{-1}$  [24]. Muonic production of  $^{36}\text{Cl}$  was calculated following Heisinger et al. [35,36]. The local production rate was calculated with scaling scheme of Stone [31]. An erosion rate of  $1$  mm per thousand years was applied. The non-cosmogenic production of  $^{36}\text{Cl}$  by neutrons from spontaneous fission of U and Th was calculated by Alfimov and Ivy-Ochs [24].

### 3. Results and Interpretation

Barhal Valley (Figures 1 and 2), called the main valley in the following, displays a distinct morphological break at  $1850$  m a.s.l. Below the break point, it has a V-shape and a narrow valley (Figure 3a), whereas it has a U-form above this point (Figure 2), and more open and broader towards the uppermost part, which is called the Hastaf Valley.



**Figure 3.** (a) View from boulder TRYAY-14 down-valley towards the gorge entrance and to the most likely ice-contact terrasses. The gorge entrance is interpreted based on the morphology and on the reconstruction of lateral ice margins (Figure 4) as the approximate LGM glacier terminus. (b) The perfectly perched erratic boulder TRYAY-14 (map position see Figure 4).

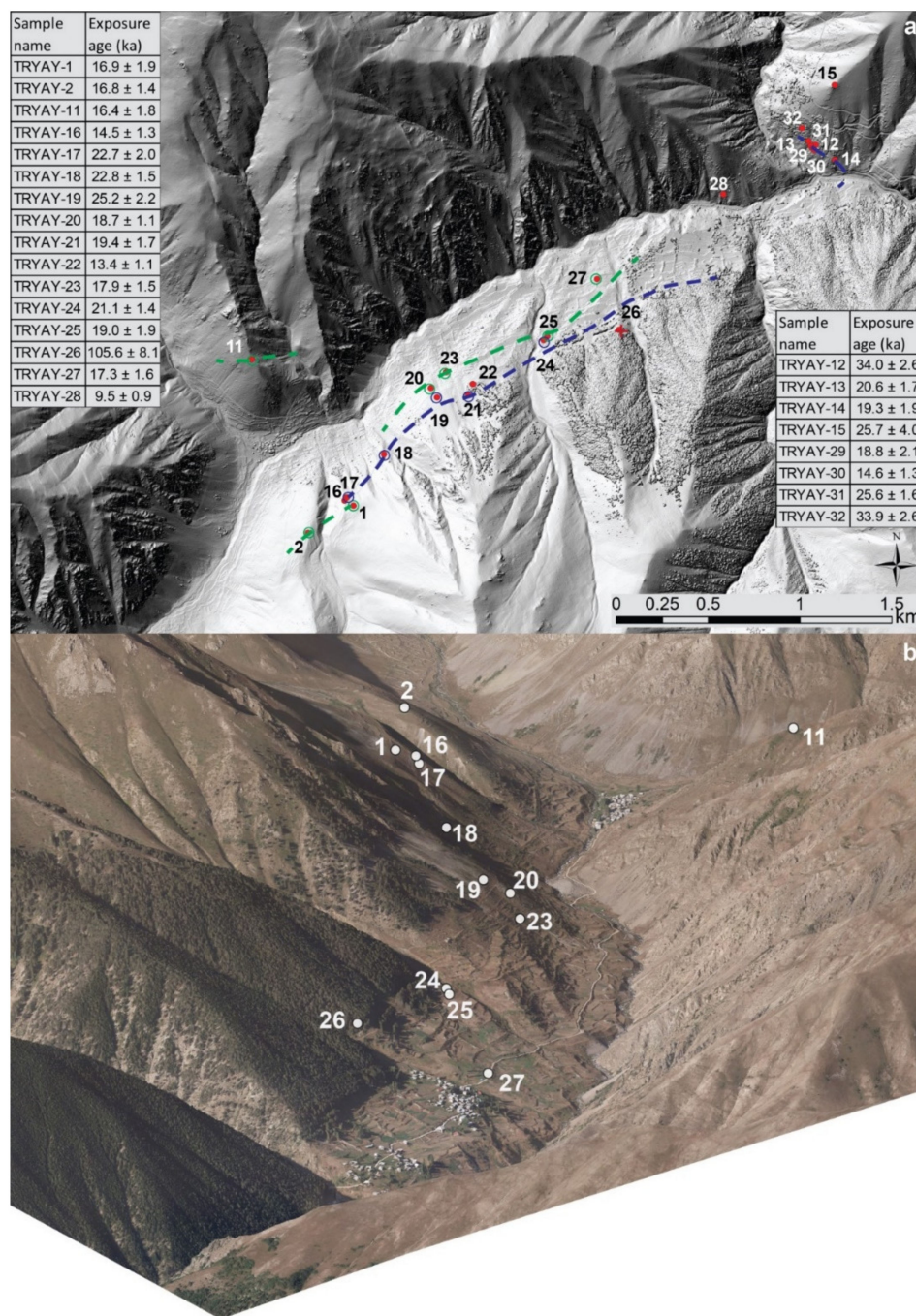


**Figure 4.** (a) Barhal Valley sample locations with summary table of cosmogenic <sup>36</sup>Cl ages. Reconstructed right lateral ice margins: lower green line = 18.3 ± 1.7 ka advance, blue line = 22.2 ± 2.6 ka advance. (b) Barhal Valley sample locations between Yaylalar (bottom of the map) and Olgunlar (at the valley confluence), as seen in digital relief reconstruction.

This break in valley morphology, from V- to U-shaped, is interpreted as the terminus of the LGM glacier (Figures 3a and 4) and, tentatively, of former glaciations as well.

The field evidence of this formerly large valley glacier with lateral relict moraine ridges, abraded bedrock surfaces, and abundant erratic boulders is omnipresent up-valley of the Yaylalar Gorge. There is a broad high alpine scenery surrounded by steep rock walls and peaks (e.g., Figure 5) in the upper Hastaf and the Dübe Valley. Glacial morphological features such as moraines or ice contact slopes are present in the main valley and rare in the tributaries of the Körahmet and Dübe valleys. There, only Lateglacial features are mapped (Figure 5).

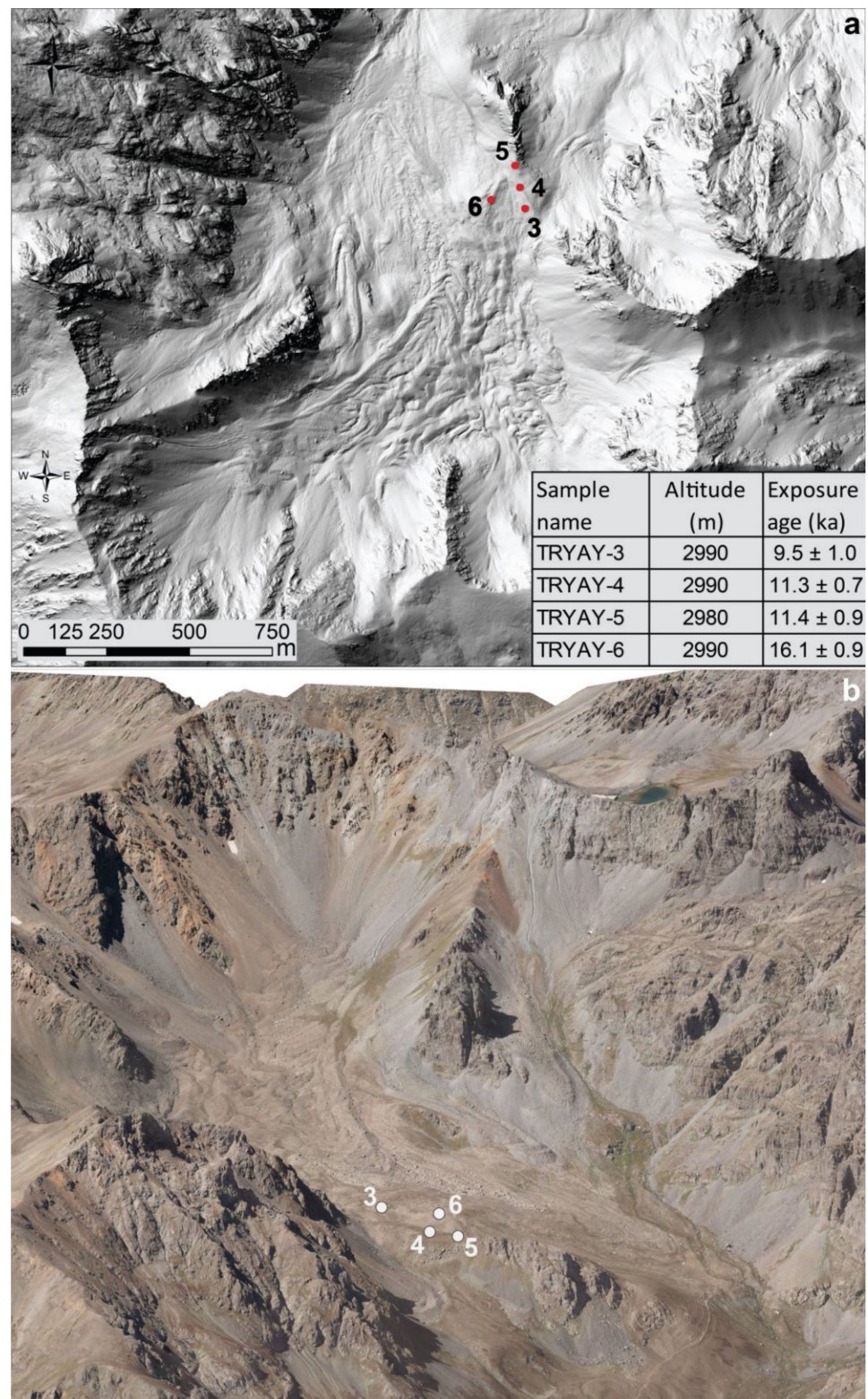


**Figure 5.** Reconstructions based on digital elevation data of uppermost Hastaf Valley with a spectacular view into the cirque to the SE of Mt. Kaçkar. (a) Detailed map with sample locations. (b) View of detailed reconstructions of land surface expressions. Samples are from areas with little periglacial modifications.

It is difficult to morphologically constrain the confluence of a paleoglacier from Körahmet valley with the main paleoglacier one kilometer upstream of the gorge entrance.

An important paleoglacial feature is at the confluence of Körahmet and the main valley on the left-lateral slope of Körahmet: it is a boulder alignment with a nicely defined upper and a more diffuse lower limit, as can be seen from Yaylalar Village (Figure 6).

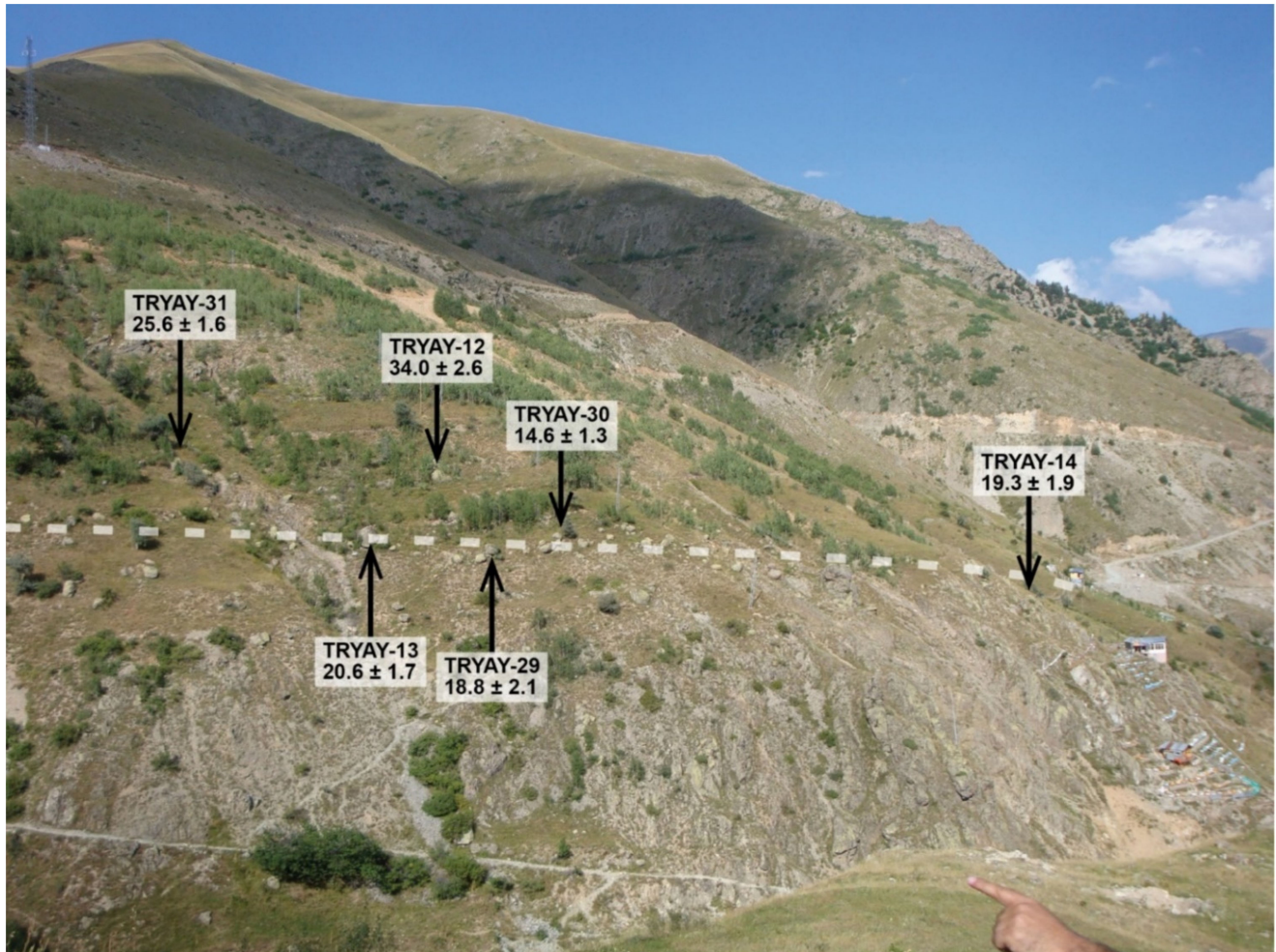


**Figure 6.** Left-lateral frontal position of Barhal Valley glacier, view to the N/NE from Yaylalar. The white line is the  $19.7 \pm 2.1$  ka ice margin. TRYAY-12 and -31 represent the  $34.0 \pm 2.3$  ka advance. For sample locations on a map, see Figure 4a. The  $18.3 \pm 1.7$  ka advance did not reach the level of the white line at that site. Details of TRYAY-14: see Figure 3.

The position of the boulders on the slope and the overall geometry at the confluence make it a depositional feature of a glacier in the main valley because the adjoining up-valley sectors of Körahmet Valley are almost free of true glacial vestiges, and the morphology is more V-shaped (Figure 1b). We conclude, therefore, that the faint boulder terrace marks the left-lateral depositional ice margin close or corresponding to the maximum glacier extension of the LGM limit of the Barhal Paleoglacier, and that the Körahmet Paleoglacier did not reach down to the main valley.

In Figures 4 and 6, the sample locations and data for the boulder alignment are given. The results of our measurements are listed in Tables 1 and 2 and Figure 6. The seven boulder samples on this slope (TRYAY-12, -13, -14, -29, -30, -31, and -32) range from  $14.6 \pm 1.3$  to  $34.0 \pm 2.6$  ka. The youngest exposure age of  $14.6 \pm 1.3$  ka (TRYAY-30) we consider as too young for a depositional age of the boulder and contemplate this surface exposure age as a post-depositional exhumation of this boulder (Table 1). Sample TRYAY-14 needs to be mentioned in particular for its methodological uniqueness and beauty (Figure 3). This boulder is delicately perched on three bedrock knobs. The boulder itself is of a subrounded form and of foreign erratic lithology. Its exposure age is  $19.3 \pm 1.9$  ka, and its position is

in the lower part of the slope. Together, TRYAY-13, -14, and -29 produce a mean exposure age of  $19.7 \pm 2.1$  ka. This exposure age allows for the decision that these samples belong to the glacier advance during the global LGM taking place at  $22.1 \pm 4.3$  ka after Shakun and Carlson, [37]. All three boulders (TRYAY-13, -14, and -29) are situated in the lowermost part of the sampled slope (Figure 6).

TRYAY-12 and -32 are of a clearly older age ( $34.0 \pm 2.6$  and  $33.9 \pm 2.6$  ka). The boulder surface of sample TRYAY-12 is slightly pitted, and the removal of the sample was easy due to embryonic spalling; this is in an agreement with the longer exposure of the boulder. A break in slope morphology below the sample TRYAY-12 is obvious. The boulders' location of TRYAY-12 is about 10 m above the upper limit of the "fresher-looking" boulder alignment, and TRYAY-32 is slightly up valley and upslope as well (Figure 3 and to the left and beyond in Figure 6). Samples TRYAY-12 and TRYAY-32 do not represent the boulder alignment in a strict sense and are considered to represent a different and older depositional age than the other samples at that site. The mean exposure age of  $34.0 \pm 2.3$  ka is older than the LGM time span for the Northern Hemisphere [37]. This is a challenging situation as it relates to the question of an Early LGM or of an older independent advance. Sample TRYAY-31 is in a similar position above the boulder line as TRYAY-12 and TRYAY-32. Its statistically significant younger exposure age of  $25.6 \pm 1.6$  ka years suggests either a later advance at around 25 ka or that this boulder was deposited with the boulder TRYAY-12 and -32, and post-depositional slope processes, not visible in the field today, are responsible for a later exhumation of this boulder. Both scenarios are possible. However, the case of deposition by a later advance at around 25 ka could explain the similar exposure ages that we find on a right lateral position farther up-valley (e.g., TRYAY-19,  $25.2 \pm 2.2$  ka, Figure 4). This would suggest a composite deposition of the till by two distinct advances at a comparable elevation in this frontal left lateral position above the LGM advance; cf. Schneebeli [38].

Sample TRYAY-15 was collected as a reference beyond and about 200 m above the boulder alignment, representing ice-free areas at the time of maximum expansion to the boulder alignment. It did produce an age of  $25.7 \pm 4.0$  ka. This age provides evidence that the higher slopes, especially this highly exposed sampled bedrock knob, may have experienced considerable erosion and "slope-cleaning"—cf. Mair et al. [39]—at the time of the glacier presence in the lower parts of the valley.

Sample TRYAY-28 was sampled because it is the only large boulder in this part of the slope (Figure 4) and was considered in the field as an up-valley extension of the boulder alignment. One should note that this boulder is resting downslope against a low bedrock ridge. The exposure age of  $9.5 \pm 0.9$  ka points to a likely post-depositional movement such as sliding and turning of the boulder since deposition; cf. Akçar et al. [15]. Therefore, we excluded this boulder from further discussion.

The intermediate sector of the southern slope of the main valley between the tributaries Körahmet Valley in the east and Dübe Valley in the west is characterized by a series of ridge segments with down-valley sloping extensions (Figures 4 and 7). These segments can be interpreted as morainic complex and ice-contact terraces. However, it is difficult to track single ridges for more than a few hundred meters down-valley. The whole slope is modified by human activity, and the clearly developed ridges have an agricultural overprint. Large boulders are elements of stability. Some are at least partially covered by gravel and small boulder fractions from land cleaning (Figure 7b,c).

Therefore, it is difficult to draw a clear limit for the extent of the paleoglacier occupying the main valley.

The sample TRYAY-26 yielded the oldest date in the valley so far with  $105.6 \pm 8.1$  ka (Figure 7d). We sampled this boulder in perspective to collect an older advance than the morphologically better constrained LGM advance. The generic higher lateral position and the decomposing-looking stage of the rounded boulder (Figure 7d) speak for an older erratic boulder sample in the field. However, the exposure age is so old that we cannot rely on this single boulder's age to propose a pre-LGM advance earlier than the 34 ka phase detected in the frontal left lateral position. To construct a much earlier advance with this

single boulder age would be highly speculative, and therefore, we conclude that TRYAY-26 contains likely inherited nuclide concentrations because of an earlier exposure in a nunatak high up in the accumulation area, which was above the LGM trimline. Therefore, this exposure age is excluded from further discussions and speculations until more evidence for such an early glacier advance is found.



**Figure 7.** (a) Down-valley view from sample station TRYAY-1 at the upper glacier margin. Note the difference in slope morphology with ice contact to the right and superficially decomposing bedrock to the left (see also Figure 7b,c). (b,c) Middle part of Barhal Valley with sampled boulders TRYAY-24 ( $22.2 \pm 2.6$  ka advance) and TRYAY-25 ( $18.3 \pm 1.7$  ka advance). (d) Sample TRYAY-26, a decomposing boulder in a steep slope affected by slope processes.

Most of the samples from the intermediate sector of the main valley can be subdivided into two groups: (1) an older age group and higher in the slope with samples TRYAY-17, TRYAY-18, TRYAY-19, TRYAY-21, and TRYAY-24, and (2) a younger age group and in lower parts of the slope with samples TRYAY-20, TRYAY-23, TRYAY-25, and TRYAY-27 (Figure 4). Sample TRYAY-17 is exposed for  $22.7 \pm 2.0$  ka, TRYAY-18 for  $22.8 \pm 1.5$  ka, TRYAY-19 for  $25.2 \pm 2.2$  ka, TRYAY-21 for  $19.4 \pm 1.7$  ka, and TRYAY-24 for  $21.1 \pm 1.4$  ka. A mean age for the older group (blue dash line in Figure 4) is  $22.2 \pm 2.6$  ka. The younger group comprises the samples TRYAY-20 with  $18.1 \pm 1.1$  ka, TRYAY-23 with  $17.9 \pm 1.5$  ka, TRYAY-25 with  $19.0 \pm 1.9$  ka, and TRYAY-27 with  $17.3 \pm 1.6$  ka, respectively. This makes an average for this group of  $18.3 \pm 1.7$  ka. Sample TRYAY-22 (Figure 4) is in a morphological position that makes it part of the younger group. Its exposure age is, however, only  $13.4 \pm 1.1$  ka; we identify this sample as an outlier, probably due to spalling as detected in the field on the lower part of the boulder but not obvious on the sampling spot.

TRYAY-1 and -2 are from boulder tops on a prominent terrace to the south of Olgunlar Village at the junction of the Dübe Valley with the main valley. Both boulders are embedded in till with characteristically striated clasts. The boulders are part of the till cover (Figures 7a and 8).

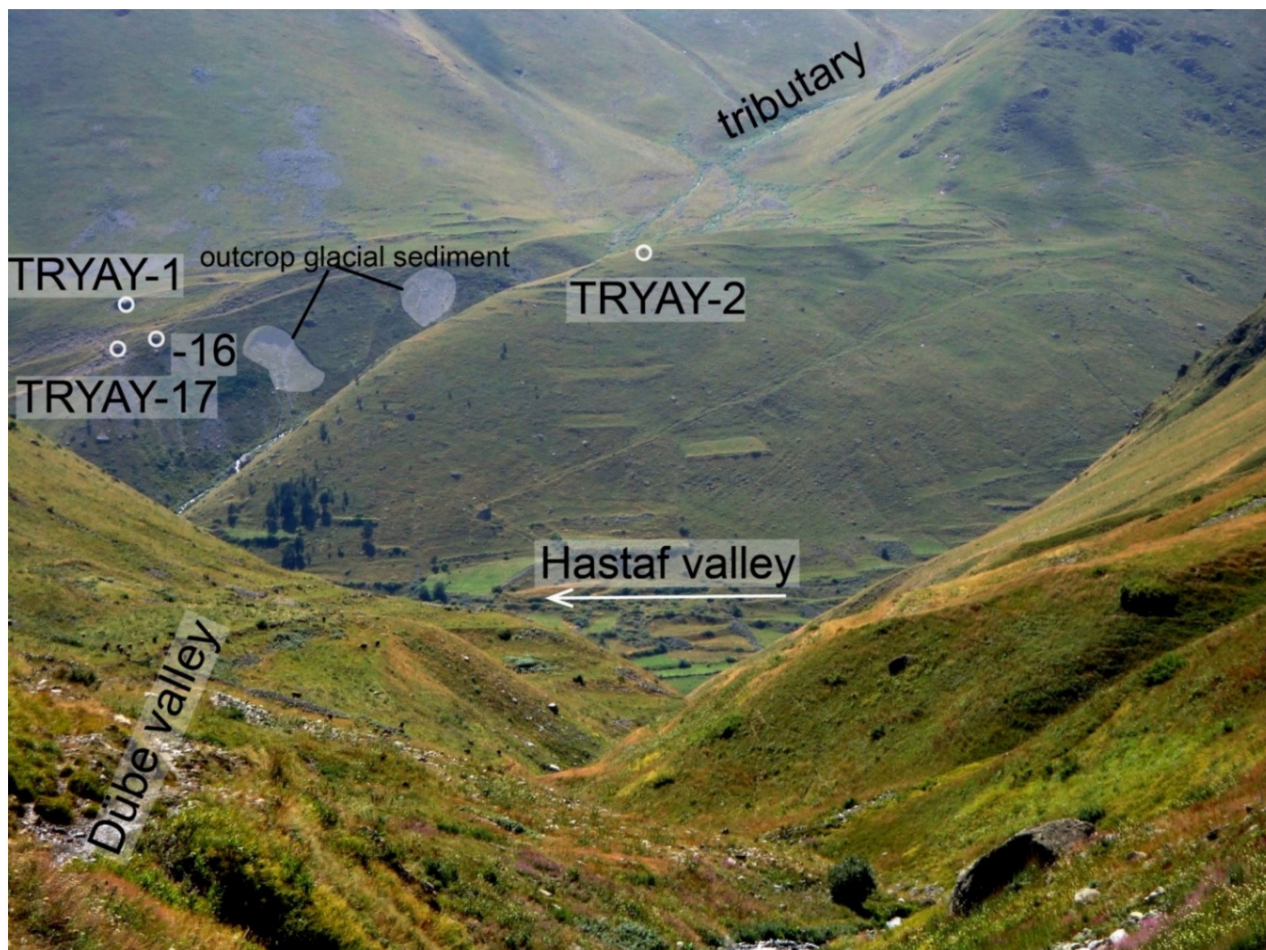


**Figure 8.** Ice contact morphologies at confluence of Dübe and Hastaf Valleys with sample and glacial sediment locations.

TRYAY-1 is on a flat terrain, and TRYAY-2 is on a ridge towards the little gully incision of the outlet from one of the smaller southern tributaries (Figures 4 and 8). Exposure ages of these boulders are  $16.9 \pm 1.9$  and  $16.8 \pm 1.4$  ka. In the northern slope above the Olgunlar Village at the entrance to Dübe Valley, abundant boulders are present. One boulder was sampled there at the comparable altitude to TRYAY-1 and TRYAY-2 at a moderately defined morphological break-in-slope, assuming that this corresponds to the ice limit of the maximum glacial extent. The exposure time of the sample TRYAY-11 is  $16.4 \pm 1.8$  ka (Figure 4). The average age of TRYAY-1, -2, and -11 is  $16.7 \pm 1.7$  ka. Based on our observations in the field, we consider the highest stand of the innermost lateral position at 2300 m a.s.l. and the continuation of this extent, mapped as a green dash-line in Figure 4, with the boulders TRYAY-20, TRYAY-23 and TRYAY-27, as a last stand still of the main valley glacier with a higher gradient of the glacier surface in this confluence area than during the earlier advance (blue dashed line with mean age of  $22.2 \pm 2.6$  ka). The average age from TRYAY-1, -2, -11, -20, -23, and -27 is  $17.7 \pm 1.9$  ka and suggests a main valley occupation by glacier ice at that time before the ice retreat toward the upper Dübe and Hastaf cirques.

However, we favor the interpretation that puts the ages of TRYAY-1, -2, and -11 with an average of  $16.7 \pm 1.7$  ka in an already ongoing down wasting phase of a glacier from

the tributary system of the Barhal Valley, and the exposure ages hint to exhumation or late deposition of the boulders in context with the stand-still or melting phase of the Dübe and smaller southern Tributary arm of the Barhal valley (Figures 4 and 8, respectively). In brief, we argue that these boulders were deposited by the tributary glacier during the down-wasting phase. With this hypothesis, the boulders TRYAY-20, TRYAY-23, and TRYAY-27 would reveal a slightly older average age from this lower green dashed line of  $18.3 \pm 1.7$  ka as reported above, and the age difference between TRYAY-1 ( $16.9 \pm 1.9$  ka) on a higher position than the older TRYAY-17 ( $22.7 \pm 2.0$  ka) could then be explained accordingly. We consider TRYAY-16 in the vicinity of these two boulders with an exposure age of  $14.5 \pm 1.3$  ka as an outlier because of the too young exposure age for this position in the valley system. In addition, a tilting of this boulder to a later stage is likely, as there are hints for this process in the field.

Well-preserved glacial landforms are rare in the upper reaches of Hastaf and Dübe Valleys (Figure 2). Between the confluence of Dübe and the main valley at about 2000 m a.s.l. and 2800 m at the entrance to the cirques, no unquestionable paleoglacier vestiges were observed. This fact is obviously the result of rapid ice down-melt and glacier retreat to the cirque area. In addition, above about 2800 m, the broad cirque floors are characterized by complex rock glaciers (Figures 5, 9 and 10).

The uppermost part of the Hastaf Valley is a broad open landscape closed by steep cirque headwalls (Figures 2 and 10a). A complex system of rock glaciers occupies the extensive cirque floors (Figures 5 and 10a,b). Morainic ridges can only be mapped with acceptable certainty in their frontal part before the valley drops off and where glacial features were not yet completely reworked by periglacial processes. A set of four samples were taken from there (Figure 5). Three samples were collected from boulders on the same ridge which marks a moderate readvance or at least a phase of ice margin stabilization. Samples TRYAY-3 with  $9.5 \pm 1.0$  ka, TRYAY-4 with  $11.3 \pm 0.7$  ka, and TRYAY-5 with  $11.4 \pm 0.9$  ka exposure time are, within errors, exposed for roughly the same period of time with a bandwidth estimation of  $11.0 \pm 1.9$  ka. It is not easy to interpret the sample TRYAY-6 from a boulder on the next ridge, which is more up-valley 90 m long with an exposure age of  $16 \pm 0.9$  ka. When considering the broader morphological context of the sampled ridges, it must be explained as most likely being the frontal part of the still-active rock glaciers, and the location was therefore subject to former rock glacier activity and boulder mixing. The interpretation of the age of sample TRYAY-6 as evidence for glacier-free cirques not later than  $16.1 \pm 0.9$  ka is a hypothesis based on this one date and therefore has to be taken with caution. TRYAY-6 could also contain inherited nuclide concentration from previous exposures at its source on the high peaks of the surrounding scenery prior to the erosion, transportation, and deposition by the glacier.

The glacial morphological configurations in the uppermost Dübe Valley are identical to the Hastaf Valley. Bedrock scenery is even more spectacular, with Mt. Kaçkar forming the high headwalls of the cirques (Figures 9 and 10c,d).

There, three boulders were sampled (TRYAY-7, -8, and -9) just outside the pronounced and most likely still active rock glaciers at the comparable altitude to Hastaf of 2900 m a.s.l., and one more sample TRYAY-10 was collected about 100 m lower in elevation. In the uppermost part, moraines are rare, and many of the rock glaciers appear to originate from remobilized glacial sediments. Samples TRYAY-7 and -8 were collected from boulders on defined ridges of several meters in height, resulting in identical exposure ages of  $15.3 \pm 1.3$  and  $15.6 \pm 1.8$  ka. Sample TRYAY-9 is from an angular rock slab on top of a ridge of a blocky moraine with thermokarst features and yielded a surface exposure age of  $12.2 \pm 1.2$  ka. This clearly younger age can be explained by the presence of thermokarst features at that location and likely represents the re-arrangement of this boulder after deposition. Therefore, we identify this boulder as an outlier and exclude it from further discussion. Several hundred meters down valley from the sample site of TRYAY-7 and on the continuation of the same ridge, the surface of a huge boulder was sampled (TRYAY-10), with the resulting age of  $14.2 \pm 1.3$  ka. We calculated a mean exposure age of  $15.1 \pm 1.6$  ka for the three boulders

from this upper region of the Dübe Valley. We conclude that this date marks the timing of glacier reorganization during the retreat in this high cirque. Based on the surface exposure dates that we gathered in the upper cirques of the Hastaf and Dübe Valley, we cannot suggest Lateglacial glacier advances. It is more likely that the exposure ages represent ice-free cirques and random morphological arrangements in the final phase of decaying glaciers at the transition to dominance by rock glaciers.

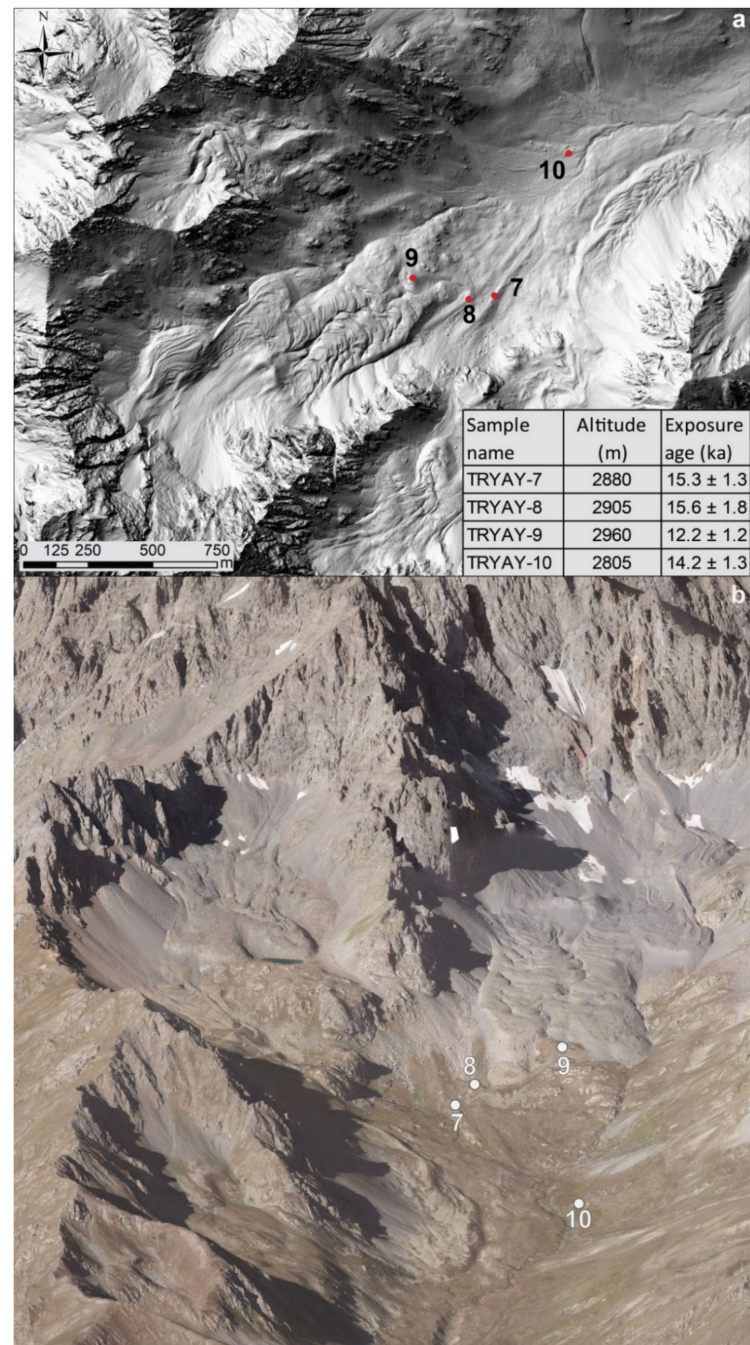


**Figure 9.** Reconstructions based on digital elevation data of uppermost Dübe Valley with a spectacular view into the cirque area of the eastern ridge of Mt. Kaçkar. (a) Detailed map view with sample locations. (b) Detailed reconstruction of the land surface expressions in the zone of contact between glacial (down-valley) and periglacial (up-valley) morphologies with delicate sample positions. Sample TRYAY-9 is from a boulder on a pronounced ridge with periglacial modifications.



**Figure 10.** Landscape and sampled boulders in the upper cirques. (a,b) Uppermost Hastaf Valley as seen from sample position TRYAY-3 and TRYAY-6, respectively. (a) View to the west with a pronounced horn morphology and with undifferentiated glacial morphologies throughout the broad cirque. (c,d) Sampled boulders and landscape in uppermost Dübe Valley.

#### 4. Discussion

In this study, we present follow-up results to our earlier investigations in northeastern Anatolian mountains: in Kavron [10], Verçenik [11], and Başyayla Valleys ([12] and Figure 1) and discuss them in a Mediterranean context (Hughes and Woodward [40], among others). Earlier investigations focused on the main valleys descending directly to the north from the high mountain ranges in the Eastern Black Sea Mountains [10–12]. The landscape above around 1800 m a.s.l. in the Kavron, Verçenik, and Başyayla Valleys are characterized by glacial morphology [9]. As stated in the introduction, the Kaçkar Mountain Range is characterized by a pronounced precipitation gradient. It has been hypothesized that this gradient also operated during the ice ages, resulting in more extensive glaciers to the north of the mountain divide than to the south in the precipitation shadow. However, paleoglaciation has been reported as well from the drier interior of the Anatolian Plateau (for instance from Mount Erçiyas; [41]), and changes in the circulation patterns during the LGM have been reconstructed for western Anatolia (Mount Uludağ; [42–44], the Balkans, e.g., [45,46]; and the Alps, e.g., [47] and references therein).

The Barhal Valley is directly descending from the eastern ridges of Mt. Kaçkar (Figures 5, 9 and 11) to the east. It is connected to the highest peak and “disappears” in the precipitation shadow as it extends to the east. Our study revealed evidence for extensive yet complex glacial features. They are morphologically poorly preserved, for example, compared to the Başyayla Valley [12].

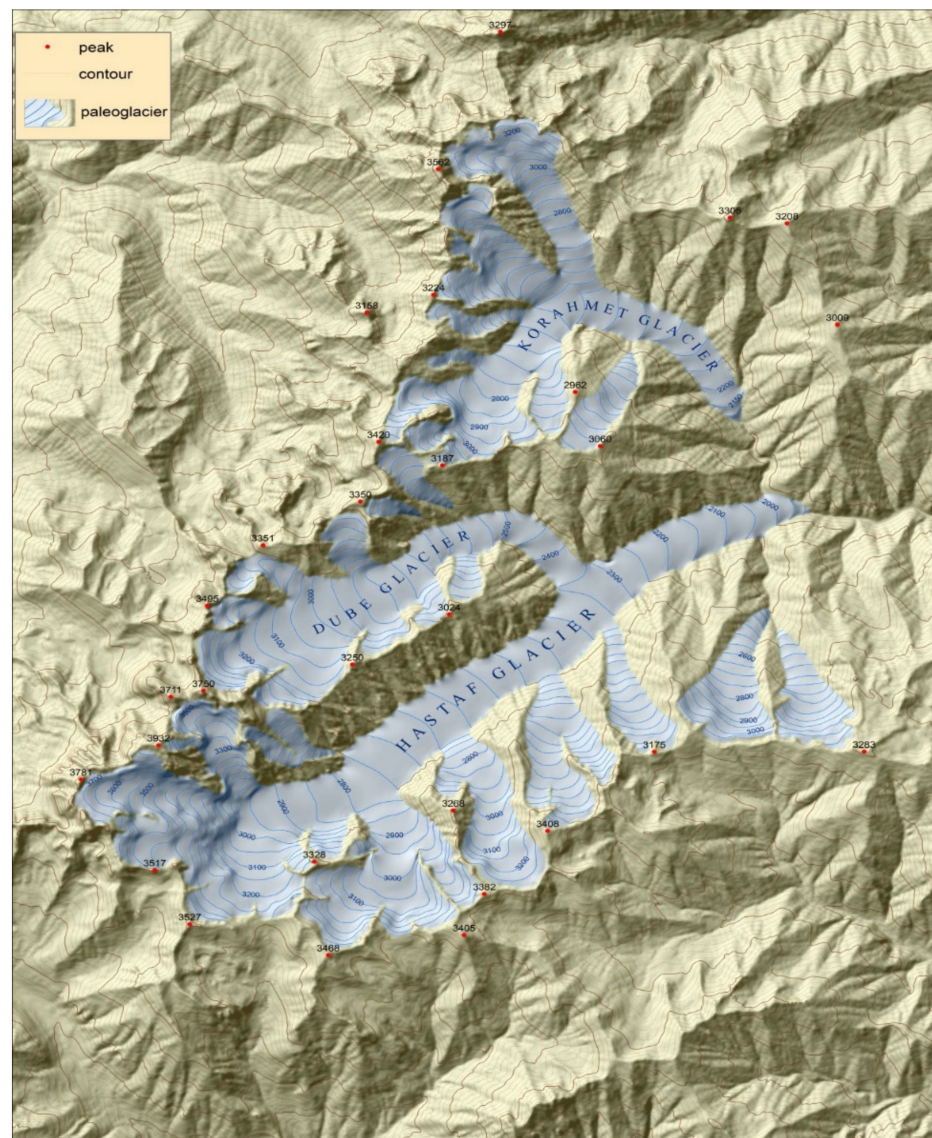


**Figure 11.** Glacier reconstruction in the Central Çoruh Valley System for the  $22.2 \pm 2.6$  ka advance. The 34 ka advance did not reach the same ice volume in the middle valley sector (Figure 3). Reconstructed maximum ELA is at approx. 2700 m a.s.l. Dube and Hastaf glaciers merged at Olgunlar (Figure 7, sample TRYAY-11). The Körachmet glacier did not reach the Barhal Valley. The reconstructed ice volume and glacier extension in the uppermost Hastaf Cirque are a first minimum approximation. Due to the Barhal Valley orientation from west to east, there are also several north-facing tributary valleys in the Hastaf Valley beside the main valley and the Dube branch. The exposition of the tributary valleys and their hypsometry probably played a considerable role in the build-up of the paleoglacier volume. Furthermore, these tributary valleys have the potential to host independent resting cirque glaciers (i.e., not connected to the glacier in the main valley) by an intermediate ELA (Equilibrium Line Altitude) depression, and therefore, they might have still been present when the main valley was ice-free after  $18.3 \pm 1.7$  ka and before  $15.6 \pm 1.8$  ka. The direct comparison of ice-covered area during the LGM of the Barhal Valley ( $34.4 \text{ km}^2$ ) to the ice-covered area of the opposing Kavron Valley ( $22 \text{ km}^2$ ) has therefore been considered with caution but still can be counted as a considerable volume.

The paleoglacier extension in the Barhal Valley is delineated by glacial morphological arguments at the gorge entrance down-valley from Yayalar (Figures 3 and 4). Additionally, less than a kilometer up-valley from the estimated glaciation limit and just at the confluence

with the Köhrahmet Valley, there is a conspicuous boulder limit in the left lateral slope. We found evidence for two glacial advances in this part of the valley, including one Early LGM with an average age of  $34.0 \pm 2.3$  ka. This glaciation is not morphologically well-constrained, but a similar advance is found in the Başıyayla Valley at  $32.6 \pm 1.3$  ka [12], as well as in the Western Taurus Mountains in the lower Kuruova Valley at  $35.1 \pm 2.5$  ka [48], which agrees with an Early LGM as proposed, for example, by Starnberger et al. [49] for the Eastern Alps. The younger glaciation detected in this frontal part of the Barhal valley is geomorphologically well-constrained with an array of boulders, and this glaciation is synchronous with the global LGM. The average age of these boulders in the frontal left lateral part is  $19.7 \pm 2.1$  ka, excluding the TRYAY-31 ( $25.6 \pm 1.6$  ka), which lies beyond two sigma uncertainty. The boulder line (Figure 6) marks a clear geomorphological break with different soil development, a stable slope surface, and an advanced vegetation cover. Accordingly, it is difficult to consider phase  $34.0 \pm 2.3$  ka just as an earlier advance of a major event also producing the  $19.7 \pm 2.1$  ka phase.

The average exposure ages of the two clusters in the middle part of the valley (blue dashed line Figure 4), with a mean age of  $22.2 \pm 2.6$  ka, and the lower ice margin (lower green dashed line Figure 4), with a mean of  $18.3 \pm 1.7$  ka, constrain the LGM advance as the main morphologically evident advances of the main valley. We propose that the Barhal Paleoglacier occupied the main valley during the period from  $22.2 \pm 2.6$  ka to  $18.3 \pm 1.7$  ka based on the ice margin evidence from the right lateral position and with a prominent phase around  $19.7 \pm 2.1$  ka when the boulder line in the left frontal position was formed.

We calculated an average age of  $21.9 \pm 2.7$  ka for the LGM in the Barhal Valley in order to compare with the existing LGM chronologies. To do so, we took the average of all 12 boulders geomorphologically attributed to the LGM (TRYAY-13, -14, -17, -18, -19, -20, -21, -23, -24, -25, -27, and -29) and excluded the Early LGM boulders (TRYAY-12, -31, and -32) and the young uppermost lateral boulders (TRYAY-1, -2, and -11 in Figure 4) from these calculations.

The amount of ice in Barhal Valley was important; the Hastaf and Dübe cirques were filled, and an ice plateau was formed at an elevation of about 3500 m, which allowed glacial landforms, such as the horns shown in Figure 10, to be sculptured by flowing ice.

A connected glacier system around Mt. Kaçkar can be postulated for the maximum LGM ice. However, it is difficult to reconstruct the Dübe Paleoglacier, as clear glacial morphologies have not yet been recognized, throughout the valley. Enormous amounts of snow must have accumulated during the LGM, as even today, snow avalanche ridges are actively formed in the valley, cf. Akçar et al. [50]. Such processes clean the high slopes from all glacial "horizontal" sedimentary landforms such as moraine ridges or ice contact slopes. The total length of the reconstructed LGM paleoglacier (Figure 11) is approximately 13 km from the farthest peak of the Hastaf Valley to the terminus. With the upper tributary of Dübe and Hastaf Valley, the reconstructed Barhal Paleoglacier has a surface area of  $34.4 \text{ km}^2$ , whereas the Dübe Paleoglacier accounts for about a quarter of this area.

We argue that the Barhal Paleoglacier reached a similar ice thickness in the middle part of upper Barhal Valley and close to identical frontal positions at the gorge entrance at around 1850 m a.s.l. during the Early LGM and LGM, as reconstructed by the stabilization phases. This position is roughly 450 m lower than the Başıyayla Paleoglacier [12]. Is this because the catchments of the cirques are broader and more effective in catching precipitation in Hastaf-Barhal, or did the eastern slope of Mt. Kaçkar receive more precipitation during the Early LGM and LGM? The broad open and flat cirque morphologies in the Barhal Valley catch large amounts of snow and ice—contrary to Başıyayla—which then descend into the funnel shape middle part of Barhal Valley, possibly explaining the advance of the glaciers to lower altitudes there.

Another important factor to compare the glacier extents of the Eastern Black Sea Mountains is the estimated modeled ELA. Based on the reconstructed extent of the Barhal paleoglacier (Figure 11), the LGM ELA was located at about 2900 m a.s.l., with an AAR (accumulation area ratio) value of 0.67. Considering Messerli's [51] estimation of the modern

ELA of about 3500 m a.s.l. in the Eastern Black Sea Mountains, we estimate an LGM ELA depression of about 600 m. Akçar [52] provided a compilation of LGM ELA depressions in the Anatolian Mountains. Accordingly, the ELA depression in the Barhal Valley is comparable with LGM ELA in the Başyayla valley, while for the directly northwards opposing Kavron Valley, the LGM ELA is estimated at 2700 m a.s.l. and the Verçenik Valley, with the estimated LGM ELA at 2800 m a.s.l. (Akçar et al. [44] and references therein). Hence, this local LGM ELA comparison reveals that the ice accumulation and glacier advance in the Barhal Valley, south of the main weather divide, are in line with its neighbors to the north of the weather divide.

The timing of the LGM advance in the broader context of Anatolia is dated at  $22.0 \pm 0.4$  (Mount Uludağ; [43,44]),  $21.5 \pm 0.4$  ka (Kavron Valley; [10]),  $20.1 \pm 1.4$  ka (Verçenik Valley; [11]),  $24.2 \pm 0.4$  (Başyayla Valley; [12]),  $> 19.2 \pm 1.2$  ka (Karçal Valley; [53]),  $20.7 \pm 2.2$  ka (Aksu Valley; [41]),  $20.4 \pm 1.5$  ka (Üçker Valley; [41]),  $19.8 \pm 0.8$  (Muslu Valley; [54]), two advances in Kartal Valley at  $22.9 \pm 3.3$  ka and  $20.6 \pm 3.1$  ka [55],  $>19.1 \pm 3.5$  ka (Namaras Valley, Geyikağ Mountains; [56]),  $20.6 \pm 0.6$  ka (Çimi Valley, Geyikağ Mountains; [57]), and  $18.9 \pm 3.3$  ka (Karagöl Valley, Bolka Mountains [58]). More details of the reported ages from Anatolia are given in Akçar [52] with a general overview. Our mean age of  $21.9 \pm 2.7$  ka for the Barhal Paleoglacier fits well in this overall picture and agrees with the global LGM that occurred at  $22.1 \pm 4.3$  ka in the northern Hemisphere [37].

The Barhal Valley is almost at the far eastern end of the Eastern Black Sea Mountains. At the western edge of the Anatolian Peninsula, there is another climatically sensitive mountain. It is Mount Uludağ, with the highest peak at 2542 m a.s.l., a mountain surrounded by lowlands. With comprehensive glacial geological mapping and cosmogenic surface exposure dating, it was possible to reconstruct timing and glacier dimensions during the LGM: maximum ice extent is dated at  $20.3 \pm 1.3$  ka, with a readvance at  $19.3 \pm 1.2$  ka [44]. These dates agree within two sigma uncertainties with the  $22.2 \pm 2.6$  ka and  $18.3 \pm 1.7$  ka phases and within one sigma uncertainty with the latero-terminal position at  $19.7 \pm 2.1$  ka in Barhal Valley.

The down-wasting of the Barhal glacier likely started shortly after  $18.3 \pm 1.7$  ka, which is marked by the lowermost set of ridges in the middle part of the main valley (Figure 4). Based on the exposure ages around  $16.7 \pm 1.7$  ka (Figure 4), one can argue that some slope stabilization and probably a reorganization of the paleoglacier system might have taken place at this time, which resulted in the disconnection of the main valley glacier from the ice tongues in the tributary valleys (Figure 11).

In the Barhal Valley, no glacial morphologies are preserved further up-valley below the periglacial landscape in the cirques. Additionally, therefore, the oldest surface exposure ages measured so far in the Hastaf-Cirque of  $16.1 \pm 0.9$  ka and Dübe-Cirque of  $15.6 \pm 1.8$  ka (Figures 5 and 10b) are interpreted to have been an ice-free cirque the latest at  $15.6 \pm 1.8$  ka. An equivalent exposure age is found in the upper cirque of Başyayla at  $17.0 \pm 1.0$  ka; cf. Reber et al. [12]. This means that the Barhal Paleoglacier disappeared within 2000 years (as in the Başyayla valley), based on the data available.

Based on the existing chronology of the glaciations in the Anatolian Mountains, we conclude that the glacier expansion during the Last Global Glacial Maximum was recorded in this peninsula in the Eastern Mediterranean, and its collapse was as rapid as in the Alps (e.g., Kamleitner et al. [47] and references therein). However, undisputable Lateglacial records are rare in the Anatolian Mountains. The rapid collapse of the glaciers during the LGM points to temperature sensitivity of the system and to an obvious rapid rise in the equilibrium line altitude.

Today, moisture transport mainly occurs directly from the Black Sea to the Kaçkar Mountains, where it rains throughout the orographic control; e.g., [6]. In a scenario with moisture transport directly from only the Black Sea, the glaciers in Kavron and Başyayla Valleys should have been gigantic with respect to the Barhal Paleoglacier. However, for equally extensive glaciers in the Çoruh valley system, as argued above, an alternative moisture source should be available. During globally cold phases, such as the LGM,

the Polar Front migrated to the south. In Western Europe, it was as far south as  $40^{\circ}$  N (Kamleitner et al. [47] and references therein), which would place it in the southern part of the Caspian Sea for the Caucasus area. Anticyclonic circulation controlled by the southerly shifted Siberian High-Pressure System causes airflow from the Aral and Caspian Sea areas across the Caucasus and westward to northeastern Anatolia, dumping precipitation on the high mountains there. The moisture feeding system in addition to the expanded Caspian and Aral seas were huge flooded areas in central Asia, as huge lakes in front of the southward expanding polar glaciers were damming the northward-flowing Siberian rivers ([59–61]; Figure 12).

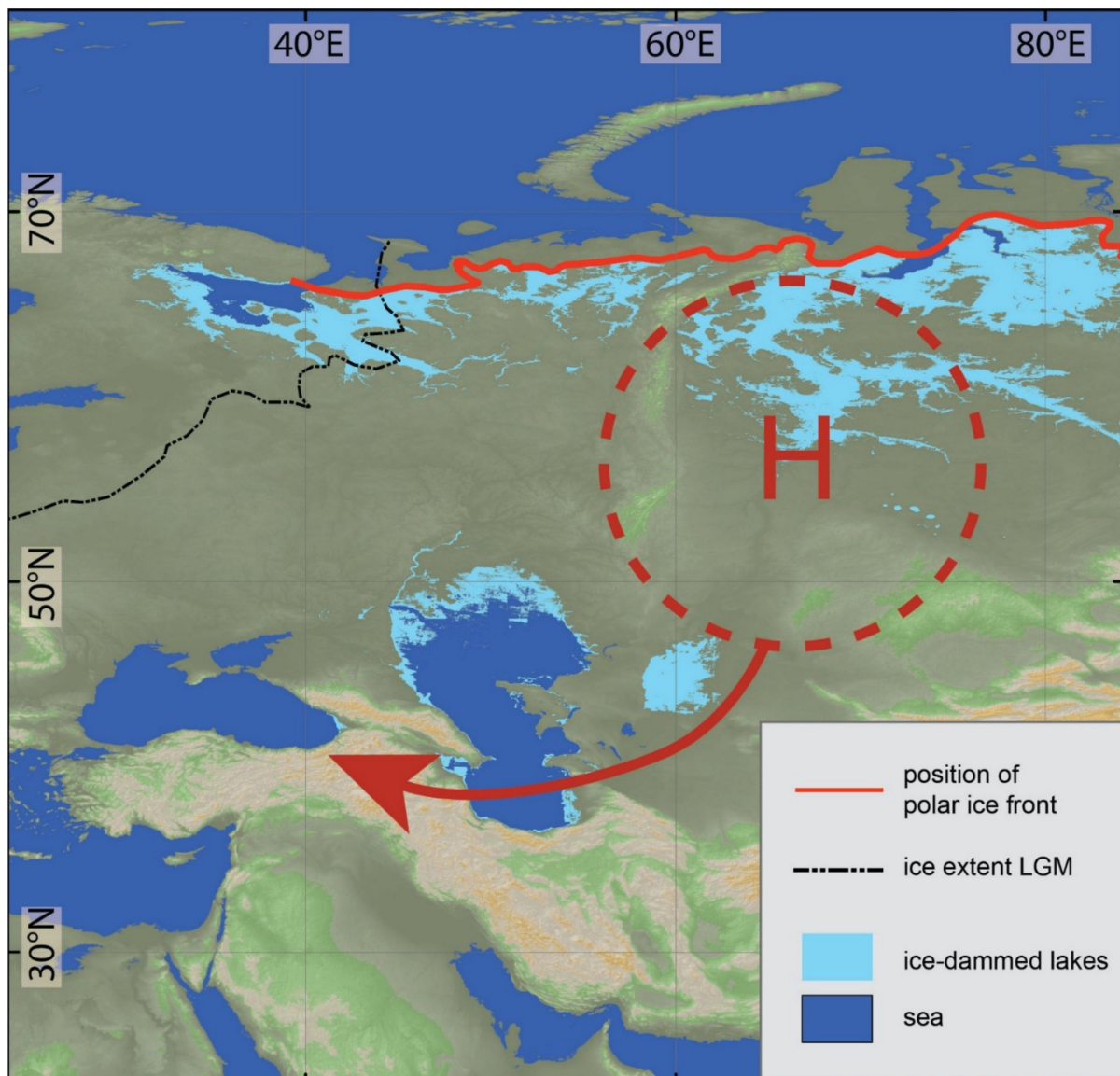


**Figure 12.** Reconstructed map of expanded water bodies between the Black Sea in the south and the White Sea in the north, modified from Mangerud et al. [60]. The age of 90 ka for this reconstruction by Mangerud et al. [60] is based on OSL dates on sediments of raised beaches, defining the large ice-dammed lakes, in this Figure calculated after Mangerud et al. [60]. This dating implies the early last glacial advance of Kara Sea ice onto the land. This chronology is under debate. Here, this reconstruction is combined with the fact that the Polar Front and, as a consequence, the Siberian High were pushed much to the south which activated northeasterly airflow to bring moisture to the Caucasian and Kaçkar Mountains from the northeast.

Available absolute age determinations on the huge Siberian Lakes, however, point to earlier damming events (and advances of polar ice onto to the continent) at 80–90 and 50–60 ka. However, these dates are not independently confirmed.

## 5. Conclusions

The field evidence in Barhal Valley favors the distinction of independent stabilization phases at  $22.2 \pm 2.6$  ka,  $19.7 \pm 2.1$  ka, and  $18.3 \pm 1.7$  ka within the global LGM and an Early LGM phase at  $34.0 \pm 2.3$  ka. The timing and expansion of these Barhal Paleoglacier extents to the south of the main weather divide are comparable to the paleoglacier extents in the neighboring valleys on the orographic Luv-side, considering the Black Sea as the main precipitation source. These findings require a more systematic comparison of glacier records from the today's Luv and Lee sides of the main weather divide in the Eastern Black Sea Mountains and the Caucasus to achieve a clearer picture of the local circulation patterns and moisture sources during glacial periods.

The deglaciation in Barhal Valley took place without stagnations producing geomorphic landmarks. The geomorphology and the exposure dates from the broad open cirque areas allow the interpretation of a complete ice retreat to the cirques at the latest at  $15.6 \pm 1.8$  ka, when chaotic ice marginal sediment aggradation with multiphase transitions to rock glacier formations and minimal morphological reorganization Figures 5, 9 and 10 interacted.

**Supplementary Materials:** The following supporting information can be downloaded at: <https://www.mdpi.com/article/10.3390/geosciences12070257/s1>, Table S1.

**Author Contributions:** Conceptualization, R.R., N.A., D.T., S.Y., C.V., V.Y., S.I.-O. and C.S.; methodology, D.T., S.Y., C.V. and N.A.; formal analysis, R.R.; investigation, R.R., D.T., S.Y. and N.A.; resources, C.S., V.Y. and N.A.; writing—original draft preparation, R.R., C.S., N.A. and D.T.; visualization, R.R. and S.Y.; supervision, C.S. and N.A.; project administration, N.A.; funding acquisition, C.S. and N.A. All authors have read and agreed to the published version of the manuscript.

**Funding:** This research was funded by the Swiss National Science Foundation Project No. 200020-125203, by the Surface Exposure Dating Laboratory, University of Bern, Switzerland, and by the Bern University Research Foundation.

**Acknowledgments:** We would like to express special thanks to the Laboratory of Ion Beam Physics operated by the Swiss Federal Institute of Technology, Zurich, Switzerland, to the Swiss National Science Foundation (Project No 200020-125203), to the Cosmolab Berne.

**Conflicts of Interest:** The authors declare no conflict of interest.

## References

1. Benn, D.; Evans, D.J. *Glaciers and Glaciation*, 2nd ed.; Taylor & Francis: London, UK, 2010; ISBN 978-0-340-90579-1.
2. Oerlemans, J. Extracting a Climate Signal from 169 Glacier Records. *Science* **2005**, *308*, 675–677. [[CrossRef](#)] [[PubMed](#)]
3. Ohmura, A.; Kasser, P.; Funk, M. Climate at the Equilibrium Line of Glaciers. *J. Glaciol.* **1992**, *38*, 397–411. [[CrossRef](#)]
4. Lukas, S.; Graf, A.; Coray, S.; Schlüchter, C. Genesis, Stability and Preservation Potential of Large Lateral Moraines of Alpine Valley Glaciers—Towards a Unifying Theory Based on Findelengletscher, Switzerland. *Quat. Sci. Rev.* **2012**, *38*, 27–48. [[CrossRef](#)]
5. Ivy-Ochs, S.; Schaller, M. Examining Processes and Rates of Landscape Change with Cosmogenic Radionuclides. *Radioact. Environ.* **2009**, *16*, 231–294.
6. Akçar, N.; Schlüchter, C. Paleoglaciations in Anatolia: A Schematic Review and First Results. *Eiszeitalt. Ggw. EG* **2005**, *55*, 102–121.
7. Türkeş, M.; Erlat, E. Winter Mean Temperature Variability in Turkey Associated with the North Atlantic Oscillation. *Meteorol. Atmos. Phys.* **2009**, *105*, 211–225. [[CrossRef](#)]
8. Climate-Data.Org. Available online: <https://en.climate-data.org/asia/turkey-67/> (accessed on 15 May 2022).
9. Akçar, N. The Anatolian Peninsula. In *European Glacial Landscapes*; Elsevier: Amsterdam, The Netherlands, 2022; pp. 149–157.
10. Akçar, N.; Yavuz, V.; Ivy-Ochs, S.; Kubik, P.W.; Vardar, M.; Schlüchter, C. Paleoglacial Records from Kavron Valley, NE Turkey: Field and Cosmogenic Exposure Dating Evidence. *Quat. Int.* **2007**, *164*, 170–183. [[CrossRef](#)]
11. Akçar, N.; Yavuz, V.; Ivy-Ochs, S.; Kubik, P.W.; Vardar, M.; Schlüchter, C. A Case for a Downwasting Mountain Glacier during Termination I, Verçenik Valley, Northeastern Turkey. *J. Quat. Sci. Publ. Quat. Res. Assoc.* **2008**, *23*, 273–285. [[CrossRef](#)]
12. Reber, R.; Akçar, N.; Yesilyurt, S.; Yavuz, V.; Tikhomirov, D.; Kubik, P.W.; Schlüchter, C. Glacier Advances in Northeastern Turkey before and during the Global Last Glacial Maximum. *Quat. Sci. Rev.* **2014**, *101*, 177–192. [[CrossRef](#)]

13. Yılmaz-Şahin, S. Transition from Arc-to Post-collision Extensional Setting Revealed by K–Ar Dating and Petrology: An Example from the Granitoids of the Eastern Pontide Igneous Terrane, Araklı-Trabzon, NE Turkey. *Geol. J.* **2005**, *40*, 425–440. [[CrossRef](#)]
14. Ketin, İ. Tectonic Units of Anatolia (Asia Minor). *Bull. Miner. Res. Explor.* **1966**, *66*, 20–37.
15. Akçar, N.; Ivy-Ochs, S.; Kubik, P.W.; Schlüchter, C. Post-Depositional Impacts on ‘Findlinge’ (Erratic Boulders) and Their Implications for Surface-Exposure Dating. *Swiss J. Geosci.* **2011**, *104*, 445–453. [[CrossRef](#)]
16. Dunne, J.; Elmore, D.; Muzikar, P. Scaling Factors for the Rates of Production of Cosmogenic Nuclides for Geometric Shielding and Attenuation at Depth on Sloped Surfaces. *Geomorphology* **1999**, *27*, 3–11. [[CrossRef](#)]
17. Reedy, R.C. Nuclide Production by Primary Cosmic-ray Protons. *J. Geophys. Res. Solid Earth* **1987**, *92*, E697–E702. [[CrossRef](#)]
18. Lal, D. In Situ-Produced Cosmogenic Isotopes in Terrestrial Rocks. *Annu. Rev. Earth Planet. Sci.* **1988**, *16*, 355–388. [[CrossRef](#)]
19. Liu, B.; Phillips, F.M.; Fabryka-Martin, J.T.; Fowler, M.M.; Stone, W.D. Cosmogenic <sup>36</sup>Cl Accumulation in Unstable Landforms: 1. Effects of the Thermal Neutron Distribution. *Water Resour. Res.* **1994**, *30*, 3115–3125. [[CrossRef](#)]
20. Phillips, F.M.; Zreda, M.G.; Flinsch, M.R.; Elmore, D.; Sharma, P. A Reevaluation of Cosmogenic <sup>36</sup>Cl Production Rates in Terrestrial Rocks. *Geophys. Res. Lett.* **1996**, *23*, 949–952. [[CrossRef](#)]
21. Phillips, F.M.; Stone, W.D.; Fabryka-Martin, J.T. An Improved Approach to Calculating Low-Energy Cosmic-Ray Neutron Fluxes near the Land/Atmosphere Interface. *Chem. Geol.* **2001**, *175*, 689–701. [[CrossRef](#)]
22. Stone, J.O.; Allan, G.L.; Fifield, L.K.; Cresswell, R.G. Cosmogenic Chlorine-36 from Calcium Spallation. *Geochim. Cosmochim. Acta* **1996**, *60*, 679–692. [[CrossRef](#)]
23. Stone, J.O.H.; Evans, J.M.; Fifield, L.K.; Allan, G.L.; Cresswell, R.G. Cosmogenic Chlorine-36 Production in Calcite by Muons. *Geochim. Cosmochim. Acta* **1998**, *62*, 433–454. [[CrossRef](#)]
24. Alfimov, V.; Ivy-Ochs, S. How Well Do We Understand Production of <sup>36</sup>Cl in Limestone and Dolomite? *Quat. Geochronol.* **2009**, *4*, 462–474. [[CrossRef](#)]
25. Schimmelpfennig, I.; Benedetti, L.; Finkel, R.; Pik, R.; Blard, P.-H.; Bourles, D.; Burnard, P.; Williams, A. Sources of In-Situ <sup>36</sup>Cl in Basaltic Rocks. Implications for Calibration of Production Rates. *Quat. Geochronol.* **2009**, *4*, 441–461. [[CrossRef](#)]
26. Akçar, N.; Tikhomirov, D.; Özkaymak, Ç.; Ivy-Ochs, S.; Alfimov, V.; Sözbilir, H.; Uzel, B.; Schlüchter, C. <sup>36</sup>Cl Exposure Dating of Paleoearthquakes in the Eastern Mediterranean: First Results from the Western Anatolian Extensional Province, Manisa Fault Zone, Turkey. *Bulletin* **2012**, *124*, 1724–1735. [[CrossRef](#)]
27. Ivy-Ochs, S.; Synal, H.-A.; Roth, C.; Schaller, M. Initial Results from Isotope Dilution for Cl and <sup>36</sup>Cl Measurements at the PSI/ETH Zurich AMS Facility. *Nucl. Instrum. Methods Phys. Res. Sect. B Beam Interact. Mater. At.* **2004**, *223*, 623–627. [[CrossRef](#)]
28. Desilets, D.; Zreda, M.; Almasi, P.F.; Elmore, D. Determination of Cosmogenic <sup>36</sup>Cl in Rocks by Isotope Dilution: Innovations, Validation and Error Propagation. *Chem. Geol.* **2006**, *233*, 185–195. [[CrossRef](#)]
29. Synal, H.-A.; Bonani, G.; Döbeli, M.; Ender, R.M.; Gartenmann, P.; Kubik, P.W.; Schnabel, C.; Suter, M. Status Report of the PSI/ETH AMS Facility. *Nucl. Instrum. Methods Phys. Res. Sect. B Beam Interact. Mater. At.* **1997**, *123*, 62–68. [[CrossRef](#)]
30. Vockenhuber, C.; Miltenberger, K.-U.; Synal, H.-A. <sup>36</sup>Cl Measurements with a Gas-Filled Magnet at 6 MV. *Nucl. Instrum. Methods Phys. Res. Sect. B Beam Interact. Mater. At.* **2019**, *455*, 190–194. [[CrossRef](#)]
31. Stone, J.O. Air Pressure and Cosmogenic Isotope Production. *J. Geophys. Res. Solid Earth* **2000**, *105*, 23753–23759. [[CrossRef](#)]
32. Evans, J.M.; Stone, J.O.H.; Fifield, L.K.; Cresswell, R.G. Cosmogenic Chlorine-36 Production in K-Feldspar. *Nucl. Instrum. Methods Phys. Res. Sect. B Beam Interact. Mater. At.* **1997**, *123*, 334–340. [[CrossRef](#)]
33. Fink, D.; Vogt, S.; Hotchkis, M. Cross-Sections for <sup>36</sup>Cl from Ti at Ep=35–150 MeV: Applications to in-Situ Exposure Dating. *Nucl. Instrum. Methods Phys. Res. Sect. B Beam Interact. Mater. At.* **2000**, *172*, 861–866. [[CrossRef](#)]
34. Stone, J. Cosmogenic Chlorine-36 Ages for the 1975 and 1984 Eruptions of Mauna Loa, Hawaii. In Proceedings of the 2005 Salt Lake City Annual Meeting, Salt Lake City, UT, USA, 16–19 October 2005.
35. Heisinger, B.; Lal, D.; Jull, A.J.T.; Kubik, P.; Ivy-Ochs, S.; Neumaier, S.; Knie, K.; Lazarev, V.; Nolte, E. Production of Selected Cosmogenic Radionuclides by Muons: 1. Fast Muons. *Earth Planet. Sci. Lett.* **2002**, *200*, 345–355. [[CrossRef](#)]
36. Heisinger, B.; Lal, D.; Jull, A.J.T.; Kubik, P.; Ivy-Ochs, S.; Knie, K.; Nolte, E. Production of Selected Cosmogenic Radionuclides by Muons: 2. Capture of Negative Muons. *Earth Planet. Sci. Lett.* **2002**, *200*, 357–369. [[CrossRef](#)]
37. Shakun, J.D.; Carlson, A.E. A Global Perspective on Last Glacial Maximum to Holocene Climate Change. *Quat. Sci. Rev.* **2010**, *29*, 1801–1816. [[CrossRef](#)]
38. Schneebeli, W. Untersuchungen von Gletscherschwankungen Im Val de Bagnes. In *Die Alpen*; Schweizer Alpen-Club: Bern, Switzerland, 1976; pp. 5–57.
39. Mair, D.; Lechmann, A.; Delunel, R.; Yeşilyurt, S.; Tikhomirov, D.; Vockenhuber, C.; Christl, M.; Akçar, N.; Schlunegger, F. The Role of Frost Cracking in Local Denudation of Steep Alpine Rockwalls over Millennia (Eiger, Switzerland). *Earth Surf. Dyn.* **2020**, *8*, 637–659. [[CrossRef](#)]
40. Hughes, P.D.; Woodward, J.C. Timing of Glaciation in the Mediterranean Mountains during the Last Cold Stage. *J. Quat. Sci. Publ. Quat. Res. Assoc.* **2008**, *23*, 575–588. [[CrossRef](#)]
41. Sarıkaya, M.A.; Zreda, M.; Çiner, A. Glaciations and Paleoclimate of Mount Erciyes, Central Turkey, since the Last Glacial Maximum, Inferred from <sup>36</sup>Cl Cosmogenic Dating and Glacier Modeling. *Quat. Sci. Rev.* **2009**, *28*, 2326–2341. [[CrossRef](#)]
42. Zahno, C.; Akçar, N.; Yavuz, V.; Kubik, P.W.; Schlüchter, C. Chronology of Late Pleistocene Glacier Variations at the Uludağ Mountain, NW Turkey. *Quat. Sci. Rev.* **2010**, *29*, 1173–1187. [[CrossRef](#)]

43. Akçar, N.; Yavuz, V.; Ivy-Ochs, S.; Reber, R.; Kubik, P.W.; Zahno, C.; Schlüchter, C. Glacier Response to the Change in Atmospheric Circulation in the Eastern Mediterranean during the Last Glacial Maximum. *Quat. Geochronol.* **2014**, *19*, 27–41. [[CrossRef](#)]
44. Akçar, N.; Yavuz, V.; Yeşilyurt, S.; Ivy-Ochs, S.; Reber, R.; Bayrakdar, C.; Kubik, P.W.; Zahno, C.; Schlunegger, F.; Schlüchter, C. Synchronous Last Glacial Maximum across the Anatolian Peninsula. *Geol. Soc. Lond. Spec. Publ.* **2017**, *433*, 251–269. [[CrossRef](#)]
45. Kuhlemann, J.; Milivojević, M.; Krumrei, I.; Kubik, P.W. Last Glaciation of the Šara Range (Balkan Peninsula): Increasing Dryness from the LGM to the Holocene. *Austrian J. Earth Sci.* **2009**, *102*, 146–158.
46. Hughes, P.D.; Woodward, J.C.; Van Calsteren, P.C.; Thomas, L.E.; Adamson, K.R. Pleistocene Ice Caps on the Coastal Mountains of the Adriatic Sea. *Quat. Sci. Rev.* **2010**, *29*, 3690–3708. [[CrossRef](#)]
47. Kamleitner, S.; Ivy-Ochs, S.; Monegato, G.; Gianotti, F.; Akçar, N.; Vockenhuber, C.; Christl, M.; Synal, H.-A. The Ticino-Toce Glacier System (Swiss-Italian Alps) in the Framework of the Alpine Last Glacial Maximum. *Quat. Sci. Rev.* **2022**, *279*, 107400. [[CrossRef](#)]
48. Sarıkaya, M.A.; Çiner, A.; Haybat, H.; Zreda, M. An Early Advance of Glaciers on Mount Akdağ, SW Turkey, before the Global Last Glacial Maximum; Insights from Cosmogenic Nuclides and Glacier Modeling. *Quat. Sci. Rev.* **2014**, *88*, 96–109. [[CrossRef](#)]
49. Starnberger, R.; Rodnight, H.; Spötl, C. Chronology of the Last Glacial Maximum in the Salzach Palaeoglacier Area (Eastern Alps). *J. Quat. Sci.* **2011**, *26*, 502–510. [[CrossRef](#)]
50. Akçar, N.; Yavuz, V.; Ivy-Ochs, S.; Kubik, P.W.; Vardar, M.; Schlüchter, C. Cosmogenic Exposure Dating of Snow-Avalanche Ridges Eastern Black Sea Mountains, NE Turkey. *Quat. Int.* **2007**, *167*, 4–11. [[CrossRef](#)]
51. Messerli, B. Die Eiszeitliche Und Die Gegenwärtige Vergletscherung Im Mittelmeerraum. *Geogr. Helv.* **1967**, *22*, 105–228. [[CrossRef](#)]
52. Akçar, N. The Anatolian Mountains: Glacial Landforms from the Last Glacial Maximum. In *European Glacial Landscapes*; Elsevier: Amsterdam, The Netherlands, 2022; pp. 497–504.
53. Dede, V.; Çiçek, İ.; Sarıkaya, M.A.; Çiner, A.; Uncu, L. First Cosmogenic Geochronology from the Lesser Caucasus: Late Pleistocene Glaciation and Rock Glacier Development in the Karçal Valley, NE Turkey. *Quat. Sci. Rev.* **2017**, *164*, 54–67. [[CrossRef](#)]
54. Zahno, C.; Akçar, N.; Yavuz, V.; Kubik, P.W.; Schlüchter, C. Surface Exposure Dating of Late Pleistocene Glaciations at the Dedegöl Mountains (Lake Beyşehir, SW Turkey). *J. Quat. Sci. Publ. Quat. Res. Assoc.* **2009**, *24*, 1016–1028. [[CrossRef](#)]
55. Sarıkaya, M.A.; Zreda, M.; Çiner, A.; Zweck, C. Cold and Wet Last Glacial Maximum on Mount Sandıras, SW Turkey, Inferred from Cosmogenic Dating and Glacier Modeling. *Quat. Sci. Rev.* **2008**, *27*, 769–780. [[CrossRef](#)]
56. Çiner, A.; Sarıkaya, M.A.; Yıldırım, C. Late Pleistocene Piedmont Glaciations in the Eastern Mediterranean; Insights from Cosmogenic <sup>36</sup>Cl Dating of Hummocky Moraines in Southern Turkey. *Quat. Sci. Rev.* **2015**, *116*, 44–56. [[CrossRef](#)]
57. Sarıkaya, M.A.; Çiner, A.; Yıldırım, C. Cosmogenic <sup>36</sup>Cl Glacial Chronologies of the Late Quaternary Glaciers on Mount Geyikdağ in the Eastern Mediterranean. *Quat. Geochronol.* **2017**, *39*, 189–204. [[CrossRef](#)]
58. Çiner, A.; Sarıkaya, M.A. Cosmogenic <sup>36</sup>Cl Geochronology of Late Quaternary Glaciers in the Bolkar Mountains, South Central Turkey. *Geol. Soc. Lond. Spec. Publ.* **2017**, *433*, 271–287. [[CrossRef](#)]
59. Thiede, J. Quaternary Environments of the Eurasian North. *Quat. Sci. Rev.* **2004**, *23*, 1225–1511. [[CrossRef](#)]
60. Mangerud, J.; Astakhov, V.; Jakobsson, M.; Svendsen, J.I. Huge Ice-age Lakes in Russia. *J. Quat. Sci. Publ. Quat. Res. Assoc.* **2001**, *16*, 773–777. [[CrossRef](#)]
61. Mangerud, J.; Jakobsson, M.; Alexanderson, H.; Astakhov, V.; Clarke, G.K.; Henriksen, M.; Hjort, C.; Krinner, G.; Lunkka, J.-P.; Möller, P. Ice-Dammed Lakes and Rerouting of the Drainage of Northern Eurasia during the Last Glaciation. *Quat. Sci. Rev.* **2004**, *23*, 1313–1332. [[CrossRef](#)]